PIEZORESISTIVE ELASTOMER SENSOR FOR ELECTRONIC SKIN APPLICATION

CHONG YUNG SIN

A project report submitted in partial fulfilment of the requirements for the award of Bachelor of Engineering (Hons.) Electrical and Electronic Engineering

Lee Kong Chian Faculty of Engineering and Science
Universiti Tunku Abdul Rahman

August 2016

DECLARATION

I hereby declare that this project report is based on my original work except for citations and quotations which have been duly acknowledged. I also declare that it has not been previously and concurrently submitted for any other degree or award at UTAR or other institutions.

Signature : _____

Name : Chong Yung Sin

ID No. : 1301033

Date : _____

APPROVAL FOR SUBMISSION

I certify that this project report entitled **"PIEZORESISTIVE ELASTOMER SENSOR FOR ELECTRONIC SKIN APPLICATION"** was prepared by **CHONG YUNG SIN** has met the required standard for submission in partial fulfilment of the requirements for the award of Bachelor of Engineering (Hons.) Electrical and Electronic Engineering at Universiti Tunku Abdul Rahman.

Approved by,

Signature : _____

Supervisor : Dr Chee Pei Song

Date : _____

ACKNOWLEDGEMENTS

I would like to express my deepest appreciation to my supervisor, Dr. Chee Pei Song for his invaluable advice, guidance and his enormous patience in the past 8 months for this research.

I would like to thank my co-supervisor, Dr. Yeoh Keat Hoe for providing the materials needed and valuable guidance in the research. In addition, I am grateful for the help from lab staffs and friends.

In addition, I would also like to express my gratitude to my family who gave me encouragement when I am in misery.

PIEZORESISTIVE ELASTOMER SENSOR FOR ELECTRONIC SKIN APPLICATION

ABSTRACT

This research is inspired by the fictitious humanoid and human arm alike prosthetic arm which able to mimic the sensing abilities by integrating a soft, flexible and stretchable human-skin alike sensor. However, the conventional sensor such as strain gauge is rigid and non-stretchable sensor which is not suitable to be implemented in e-skin. Recent advancement in micro electro-mechanical system (MEMS) fabrication technology has enabled the fabrication of this fictitious electronic skin e-skin to sense static and dynamic pressure, detect temperature change and stretchable. E-skin in this project quantifies touch sensing by utilising the piezoresistivity mechanism of conductive elastomer material under deformation. Conductive elastomer material of e-skin comprises non-conducting polymer, polydimethylsiloxane (PDMS) and conductive filler, multiwall carbon nanotubes (MWCNT). Piezoresistivity of this e-skin attributed to the connection of tunnelling resistance or quantum tunnelling conduction between fillers, reformation of the percolating path. Tactile sensing ability and stretchability were studied using finite element analysis (FEA) using COMSOL Multiphysics. Fabrication of the e-skin was carried out by micromolding the polymer composite into a matrix structure PDMS mold and serpentine structure photoresist mold. The fabricated e-skin shows a resistance change upon subjected to static and dynamic pressure, strain and temperature variation.

TABLE OF CONTENTS

LIST OF TABLES

LIST OF FIGURES

LIST OF SYMBOLS / ABBREVIATIONS

P	pressure, kPa
R	resistance, Ω
T	temperature, ˚C
ρ	density, kg/m^3
ν	Poisson's ratio
ε_r	Relative permittivity
E	Young's modulus, Pa
DMM	digital multimeter
DUT	device under test
DWCNT	double-wall carbon nanotube
FEA	finite element analysis
FOTS	trichloro(1H,1H,2H,2H-perfluorooctyl)silane
MEMS	micro-electro-mechanical system
MWCNT	multiwall carbon nanotubes
PDMS	polydimethylsiloxane
Si	silicon
SWCNT	single-wall carbon nanotube

CHAPTER 1

INTRODUCTION

1.1 Background

Sensor is a kind of transducers which able to detect the changes in phenomena or environment and convert the input signals into the other kind of signal. Signal which transduced from the sensor (mostly analog signal) is converted into electrical signal (by ADC) to interface with digital circuitry. As an example, the signal received from the thermocouple is sent to a signal conditioning circuit which interfaces with ADC before it is passed to a microcomputer for further interpretation. Nowadays, a lot of microscopic scales actuators and sensors are designed based on a technology called micro-electromechanical system (MEMS) which is inspired by IC technology. MEMS is an emerging technology starting from 20th century due to the demand of miniaturization of devices (Liu, 2011).

Human skin is the largest organ in the integumentary system. Most of the sensory units are embedded beneath human skin. It covers the outer layer of human body to provide physical protection from the outer environment. It not only function as a physical protection but it also allows us to sense different parameters such as temperature, static and dynamic pressure, shapes and texture of contacted surface. Receptors which integrated under human skin is first transduced physical information into electrical signals and send to the brain, which is part of the central nervous system to interpret received data by somatosensory cortex (Hammock et al., 2013). Mechanoreceptors which respond to static and dynamic pressure are Merkel

and Ruffini corpuscles and Meissner and Pacinian corpuscles respectively (Park et al., 2015).

1.2 Problem Statement

Electronic skin (e-skin) is an artificial skin alike sensor which engineered for sensing abilities as human skin does, including the ability of self-healing. However, most of the existing MEMS sensors such as strain gauge are fabricated using non-flexible materials (such as silicon and copper) which have limited its integration to dynamic moving surface. Hence, elastomeric polymer is chosen by most of the researches in implementing e-skin, due to its flexible and viscoelastic behaviour with soft sensation compares to the conventional nonflexible silicon MEMS (Liu, 2011). It is either integrated with conductive fluids using microfluidic approach or conductive fillers in a polymer to employ the change in electrical properties. In this project, poly-dimethylsiloxane (PDMS) is chosen to be incorporated with multiwall carbon nanotubes (MWCNT) as the conductive fillers to implement e-skin after comparing with the other possible materials in term of cost, fabrication process, availability of materials and equipment, electrical and mechanical properties of materials.

E-skin realization is promising by using piezoresistive elastomeric composite due to its chemically inert properties, inherent elasticity, and simple, scalable, and relatively cheaper fabrication method. Piezoresistivity change is attributed to the changing tunnelling resistance caused by the changing filler distance when the composite subjected to external deformation (Park et al., 2014a). It is further optimized by controlling the weight percentage of the composite near the percolation threshold.

1.3 Aim and Objectives

The major aims of this project are design and fabricate an e-skin sensor using elastomer material operated based on piezoresistivity mechanism. This sensor is used to detect normal force, pressure distribution on the e-skin, shear force, stretching and temperature. As an ultimate goal, this project is carried out to pursue an e-skin prototype which able to sense multi parameters in a single unit which is better than conventional non-stretchable and single function sensor.

Objectives which set to achieve the aim as stated are shown as following:

- To design and fabricate a stretchable e-skin prototype using piezoresistive principle.
- To characterise the developed e-skin with the function of static and dynamic compression, strain and temperature

1.4 Report Overview

This report is structured as followed: Chapter 2, the literature review on the history of current e-skin development, implementation methods and materials for piezoresistive e-skin, pros and cons on the existing design and parameters which affect e-skin sensitivity during the fabrication process. The methodology will be covered in Chapter 3 to explain the analysis on the result of the e-skin structure using Finite Element Analysis (FEA), method of fabrication for e-skin, and characterization methods and parameters for e-skin. After that, the results of fabrication, FEA and device characterization will be presented in Chapter 4. Finally, conclusion will be drawn in Chapter 5 and future works about ideas and recommendations to improve the performance of current prototype.

CHAPTER 2

LITERATURE REVIEW

2.1 History of E-skin

Human skin is a common organ which many people tend to neglect the beauty of this sensory organ. E-skin has now become a hot topic in the field of sensor research. According to an article written by Zhenan Bao Research Group from Stanford led by Zhenan Bao (Hammock et al., 2013), the idea of e-skin was originated from science fictions which published from 1970s to 1990s.

It was believed that artificial organs which used for human body replacement were inspired by a science fiction, 'Caidin's Cyborg' in 1971 and was then filmed as 'The Six Million Dollar Man TV series' in 1974 (Harve, 2002). Subsequently, an epic scientific movie series, Star Wars which screened in 1977 also envisioned the application of e-skin. One of the characters in the movie, Luke Skywalker has installed a sensors integrated prosthetic arm after losing his arm in a battle. Moreover, the self-healing ability of e-skin also an attractive feature which can be found in the Terminator movie series in 1984, that robot was able to heal themselves (Hammock et al., 2013).

At the same time, e-skin development has also been initiated by the advancement of microelectronics and semiconductors. Clippinger et al. have demonstrated a prosthetic arm which integrated with discrete sensors in 1974 (Hammock et al., 2013). Almost a decade later, HP has commercialized a personal computer (HP-150) with the touchscreen display. General Electric has built an

infrared based e-skin on a stretchable material for robotic arm usage with the resolution of 5cm. This prototype had demonstrated its sensitivity towards the environment as it move effectively and avoid obstacles. This has made the interaction between a human and a machine possible as no pre-programmed motions was set on the robotic arm to put up a ballet dance (Hammock et al., 2013).

Furthermore, the scientists have approached for a cheap, large area and printable of sensor sheets using flexible electronics materials in the 1990s. The first flexible sheet using Si-Micro-electro-mechanical island which etched from thin Si wafers is presented by Jiang et al. and islands were integrated on a flexible polyimide foils (Hammock et al., 2013). It shows the improvement of tactile and shear force sensing ability and mechanical deformation ability. Nearly the same time, fabrication of flexible array using organic semiconductor materials has demonstrated its potential to replace amorphous Si. Right before the age of millennium, NSF and DARPA have collaborated to organize a sensitive skin workshop which held in Washington D.C., it has attracted researchers in academy, industry and government. The significant industrial interests were shown in e-skin applications including robotics sensing features and health monitoring system.(Hammock et al., 2013)

Starting from the 2000s, researchers began to search for various types of sensors that are able to integrate with the microcomputer and accentuate on mimicking the mechanical properties and human skin's sensitivity. Development of stretchable electrodes was presented by Suo and co-workers (Lacour et al., 2003). Besides, Rogers and co-workers have developed a Si-based stretchable high-performance electronics using ultra-thin films (around 100 nm) interconnected by flexible materials. Moreover, stretchable pentacene based OFET for wide area pressure sensing sheets with matrix readout mechanism and novel pressure sensing sheet using integration of FET with foam dielectric and ferroelectrets were presented by Someya with co-workers and Bauer with co-workers respectively. Moreover, Bao's group has demonstrated high sensitivity of micro-structured elastomeric dielectrics and self-healing conductive elastomer composite with mechanical pressure sensing ability. Developments in area including e-skin integrated with LED and organic photovoltaics (OPV) cell is now under intensive research. Figure 2.1 shows the chronological timeline of e-skin development (Hammock et al., 2013).

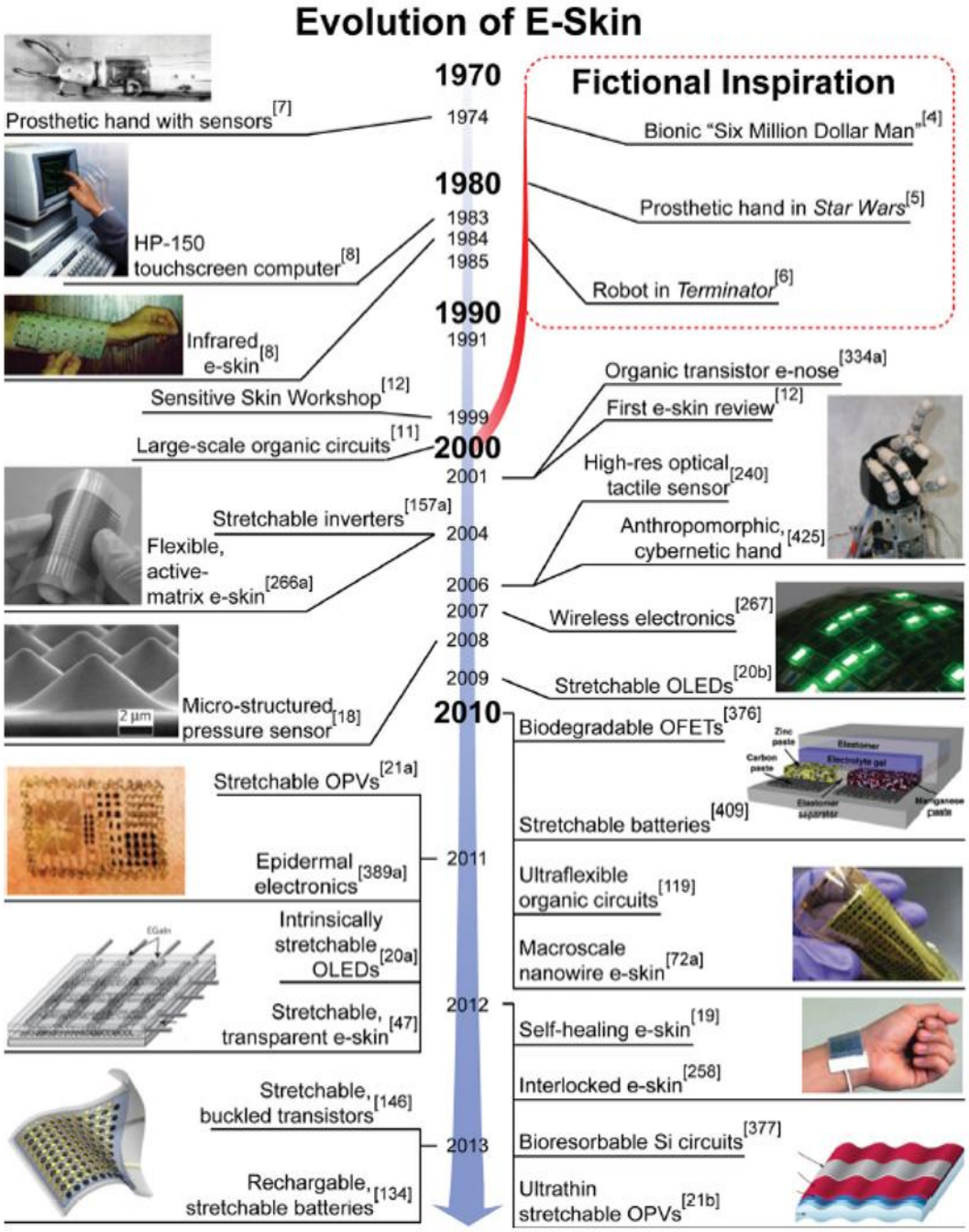

Figure 2.1 Timeline of E-skin Development (Hammock et al., 2013)

2.2 Transduction Method

2.2.1 Capacitive Transduction

Capacitance of a parallel plate capacitor, C is determined by the relative permittivity, ε_r, cross sectional area of the plate, A, and inter-plate distance d. According to research (Hammock et al., 2013), d is used to differentiate normal force exerted on the sensor, A are dedicated for shear force detection and ε_r is specifically for force detection by materials which has electrostatic charge induced (Fan-Gang et al., 2004). The main advantages of this transduction method are device design, analysis method is easy because it is governed by 3 parameters, durable when it is subjected to high tensile force, ability to detect static force, and low power consumption. Materials implemented in e-skin such as Ecoflex® silicone as dielectric of sensor, stretchable electrodes using CNT, nanowires and Au inter-fillers. However, it has its limitation due to the incompressible and viscoelasticity of rubber material. To overcome this problem, air gaps can be introduced to increase the flexibility of sensors with trade-off of lowering C and low signal to noise ratio. Sensors which are worked under capacitive transduction method are shown in Figure 2.2.

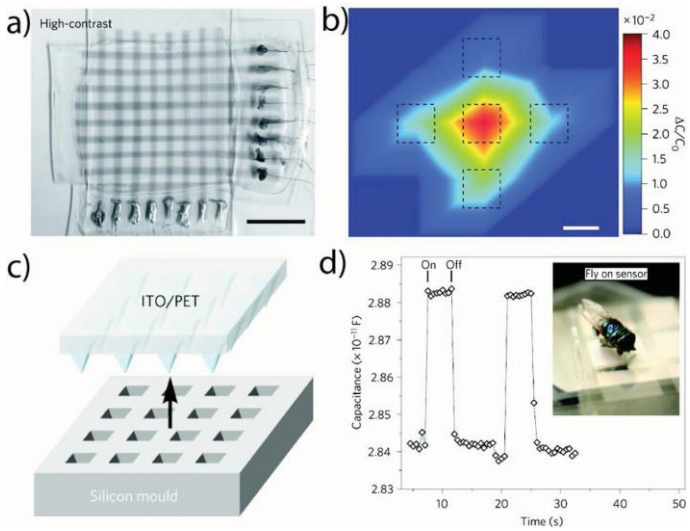

Figure 2.2 a) Capacitive E-skin Sensors with Matrix Array Readout. b) Pressure Distribution Image which Induced by External Pressure c) Fabrication of Sensor with Pyramidal Array Pattern. d) Sensitivity Test when attached with an Approximately 20 mg of Fly and Land on E-skin. (Hammock et al., 2013)

2.2.2 Optics

Optical transduction method works under the same principle as photodetector which convert light signal to electrical signal. It receives feedback by the integrated light source through a light-guide as the transmission medium, including force-sensitive lightguides and flexible optical fibres. Figure 2.3 a) shows the principle of operation of an optical based tactile sensor which presented by Z. Bao et al (Hammock et al., 2013). This device has pressure sensitive of 0.2 kPa^{-1} and it able to detect the application and removal of 30mg of weight. Besides, a large area sensor is employed in Koeppe et al. which detect light signal that has outcoupled from elastomer lightguide due to the deformation of transmission pathway as shown in Figure 2.3 b) (Hammock et al., 2013).

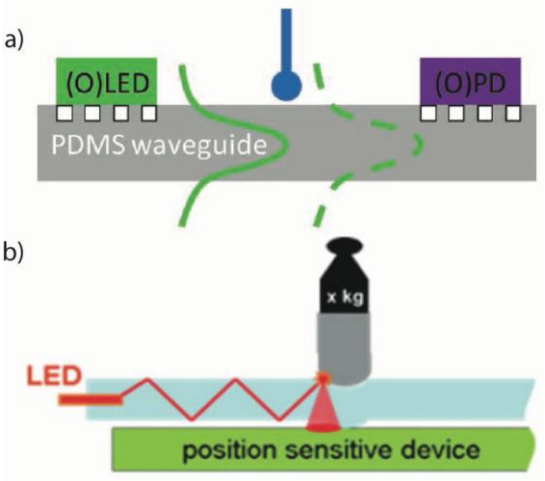

Figure 2.3 a) Optical based Tactile Sensors that Modulate Light Signal through PDMS Waveguide. b) Light Signal which Coupled to the Stretchable Waveguide is sent to Array of Detectors. (Hammock et al., 2013)

2.2.3 Piezoresistivity

Piezoresistive based sensor is intuitive as its name that resistance of the material varies when pressure applied upon it. Resistance is generally the measurement of electron mobility in certain materials. Hence, parameters such as geometry variation of material, bandgap of the materials dominates resistivity of materials, linkage of

resistance between different materials and the inter-particle separation of material. Figure of merit for a strain sensor is determined by gauge factor and it is governed by fraction of change in resistance over the strain experienced by the material. Normally, mobility decreases when strain is applied because of wider intermolecular or intergrain separation than original (Hammock et al., 2013).

Mechanisms have been found to achieve piezoresistivity in composite materials including band structure variation, connections of tunnelling resistance between fillers and reformation of percolating pathway. In contrast to stretchable conductor, it has the optimum performance when the composite is loaded with filler at the percolation threshold. This is because piezoresistivity or electrical conductivity will change sharply when the composite deformed especially at percolation threshold. Figure 2.4 shows that the conductivity gradient at point c is much steeper than a, b and d, (Alamusi et al., 2011).

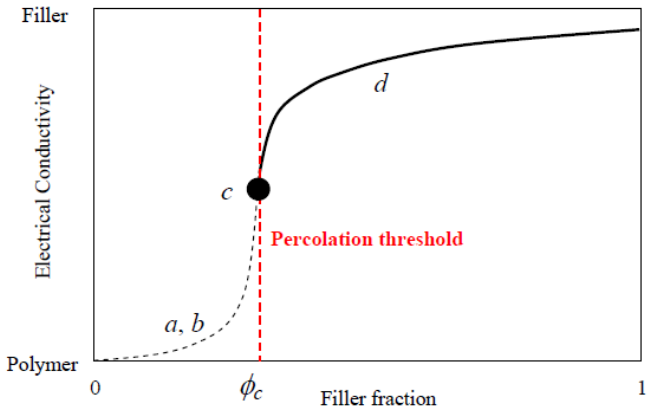

Figure 2.4 Electrical Conductivity of Conductive Composite versus Filler Fraction (Alamusi et al., 2011)

Conductive filler in elastomeric composite which has been used to fabricate this e-skin including, CNT, carbon black and metal particles. Metal fillers type of piezoresistive composite has been commercialized by Pratech Ltd. due to the prominence performance in focusing electric field for better tunnelling current when pressure exerted on it. (Hammock et al., 2013)

2.2.4 Piezoelectricity

Piezoelectricity is the properties of a material which able to generate the voltage when it is subjected to applied force. This is because the force applied on the materials will cause the separation between a pair of charges hence leading to building up of compensating charges. The dominating factor that determine its quantity is piezoelectric strain constant (d_{33}) of the material (Hammock et al., 2013). Besides, Pyroelectric mechanism that explains the behaviour of voltage change that induced from temperature change also can be found in piezoelectric material. It has a huge potential to be used in e-skin because piezoelectric and pyroelectric behaviours shown in human skin (Park et al., 2015). Therefore, it is able to reflect any variations in temperature and pressure at the same time, using a single sensor.

Dispersion of inorganic particles such as reduced graphene oxide (rGO), lead zirconate titanate (PZT) into polymer especially Polyvinylidene difluoride (PVDF) are the ideal materials for this sensor. PVDF is widely used because of its d_{33} coefficient and stretchability is much lower and better than normal ceramic materials. A ferroelectric properties e-skin with microdome array interlocked structure has been demonstrated by Park et al. with remarkable static and dynamic pressure, temperature and vibration detection (Park et al., 2015) as shown in Figure 2.5.

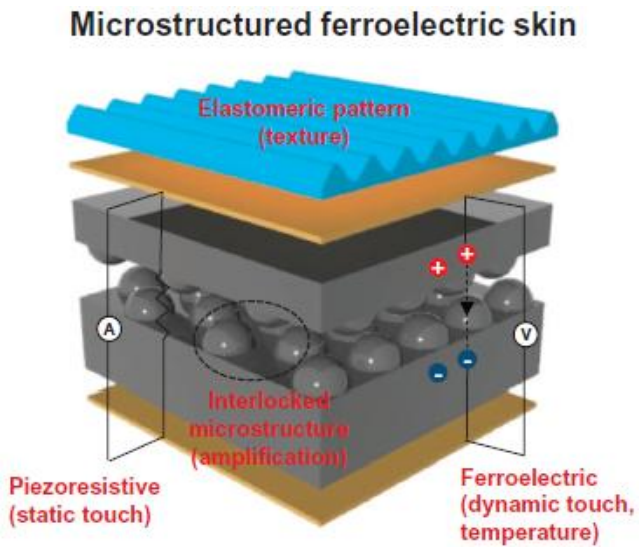

Figure 2.5 A Stretchable and Multimodal Ferroelectric E-skin. (Park et al., 2015)

2.2.5 Wireless Antenna

Antenna is an electrical device which acts as a receiver or transmitter through receiving or transferring of electromagnetic waves. It is normally used to power up devices, however, Whitesides and co-worker have presented flexible radiofrequency antenna when pressure applied upon it which shown in Figure 2.6. (Kubo et al., 2010)

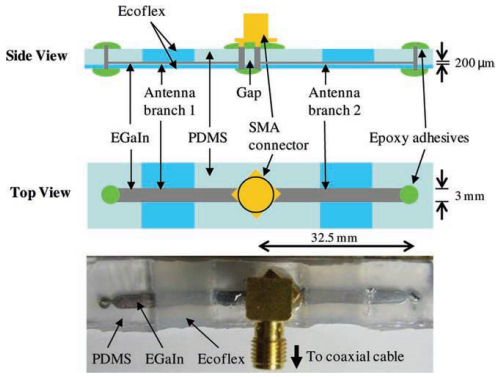

Figure 2.6 A Stretchable Antenna using Microfluidic Approach (Kubo et al., 2010)

The working principle is the antenna will change its resonant frequency (from 1.53 to 0.738 GHz) when the sensor is deformed (from 0 to 120% strain) using PDMS/CNT-based materials with the microfluidic approach (Kubo et al., 2010). Moreover, it has been used to measure pressure in a chamber remotely which attributed to its wireless connection (Tang et al., 2012).

2.3 Materials for Piezoresistivity Based E-skin

2.3.1 PDMS (Elastomeric Materials)

PDMS is a type of room temperature vulcanized silicon elastomeric material which able to recover even large deformation is exerted (Liu, 2011). Among polymers including poly(methyl methacrylate) (PMMA), polycarbonate (PC), polyethylene (PE). PDMS has advantages of chemically stable, temperature stability, transparent,

mechanically elastic properties and viscoelasticity variable characteristics controlled by UV radiation (Liu and Choi, 2012). In addition, PDMS offered higher sensitivity, low delay time and cheap in cost (Tai and Yang, 2015).

In term of mechanical behaviour, it is able to withstand more than 100% of threshold deformation stress easily. Besides, it is a desirable dielectric material for applications especially flexible transistors and capacitive based tactile sensor. This is attributed to its high dielectric constant and low leakage currents (Hammock et al., 2013). Moreover, it has been widely used by researchers in lab-on-a-chip (LOC) system especially microfluidic devices such as micromixers, microchannels, micropump, microvalve and parts for connection (Khosla and Gray, 2009).

2.3.2 CNT (Conductive Fillers)

CNT has drawn attention by researches started from its discovery in 1991 especially in nanoelectronics fabrication due to its remarkable electronic and chemical stable mechanical properties. There are different methods that can be used in synthesising CNT such as arc-discharge, laser ablation and catalytic CVD to yield MWCNT or single-wall carbon nanotube (SWCNT) or double-wall carbon nanotube (DWCNT). CNTs can also be portrayed as the rolling layer of graphene which made of planar hexagonal shaped layer of carbon-carbon bonds. The main difference between them is the number of layers (Bokobza, 2007).

Excel electrical behaviour is contributed by near ballistic transport for CNT without defect with carrier mobilites up to 10,000 $cm^2V^{-1}s^{-1}$ for SWCNT (Hammock et al., 2013). Polymers which consists of CNT fillers has great potentials to be used in electronic's materials such as organic LED, photovoltaic cells and sensitive tactile sensors. Its aspect ratio, length, L over diameter, D governed the percolation threshold of the polymer composite when formation of percolating pathway governs the piezoresistivity of materials (Alamusi et al., 2011). Besides, it has been noticed that MWCNT has better conductivity and cheaper in cost than SWCNT (Liu and Choi, 2012).

2.4 Structural Design and Stretchability Strategies

2.4.1 External Bumped Surface

Arrays of devices are enclosed within an elastomer to isolate it from external mechanical damage and environmental exposure. This method has the disadvantages of reducing resolution and sensitivity of the device as hysteresis was observed in pressure detection. A bumped surface or force localising protrusion (FLP) is created on the surface of sensor. It acts similarly as the intermediate ridges between epidermis and dermis of human skin. It is also able to detect either normal or shear force exerted on it by converting it to tensile force or normal force respectively. Figure 2.7 shows a single FLP on the surface of tactile sensor (Hammock et al., 2013).

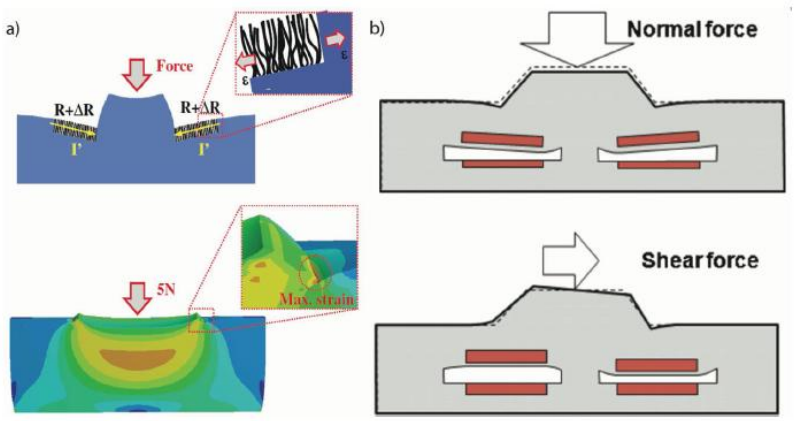

Figure 2.7 a) Strain and Pressure Distribution on FLP Structure Tactile Sensor. b) Normal Force and Shear Force Detection. (Hammock et al., 2013)

2.4.2 Multitude Stimuli Sensing with Microdomes or Micropillars

Microdomes or micropillars design aimed to detect multiple sensations as human skin does such as normal, shear and torsional force, temperature, pH and air flow. In 2012, Pang et al. has demonstrated a stretchable and multitude detection piezoresistive e-skin using interlocking nanofibers structure. The inspiration of this design is originated from the machanotransduction systems in nature including

cochlea hair cells, microvilli in intestine and kidney. It operates based on external forces applied on it causing increase and decrease in contact of nanofibers hence contact resistance made of high polyurethane acrylate (PUA) coated with platinum (Pt) electrodes. This design able to detect the type of force exerted based on the resistant change vs time and applied strain signal vs time graphs. Figure 2.8 shows the design of the e-skin.

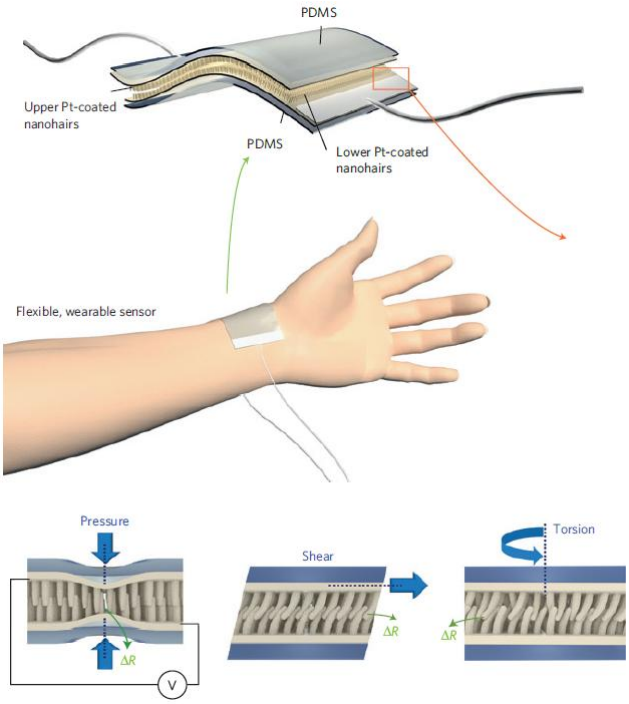

Figure 2.8 Piezoresistive E-skin using Interlocking Nanofibers Structure (Pang et al., 2012)

Subsequently, improvement in micropillar design was presented by Park et al. in 2014 e-skin with interlocking microdome arrays by using CNT/PDMS polymer composite materials. This design is inspired from fingertip's epidermis and dermis ridge which is believed to be the most sensitive sensing region of human body. Its high sensitivity in recognition of normal, shear and vibration individually has been reported and multitude stimulus also can be detected by it. Hence, this design was further optimized in aspect including height, diameter, and pitch of the microdome arrays. It has been concluded that the smaller pitch or inter-distance of micropillar, smaller diameter of micropillar can reaches higher sensitivity. Pyramidal array has been identified with the similar dimension of micropillar and it shows improvement

in response time and relaxation time. However, it shows a less sensitive behaviour for pressure less than 0.1 kPa due to less MWCNT located at the tip of pyramid. Figure 2.9 shows the micropillar structure CNT/PDMS based piezoresistive e-skin. (Park et al., 2014a, Park et al., 2014b, Park et al., 2014c).

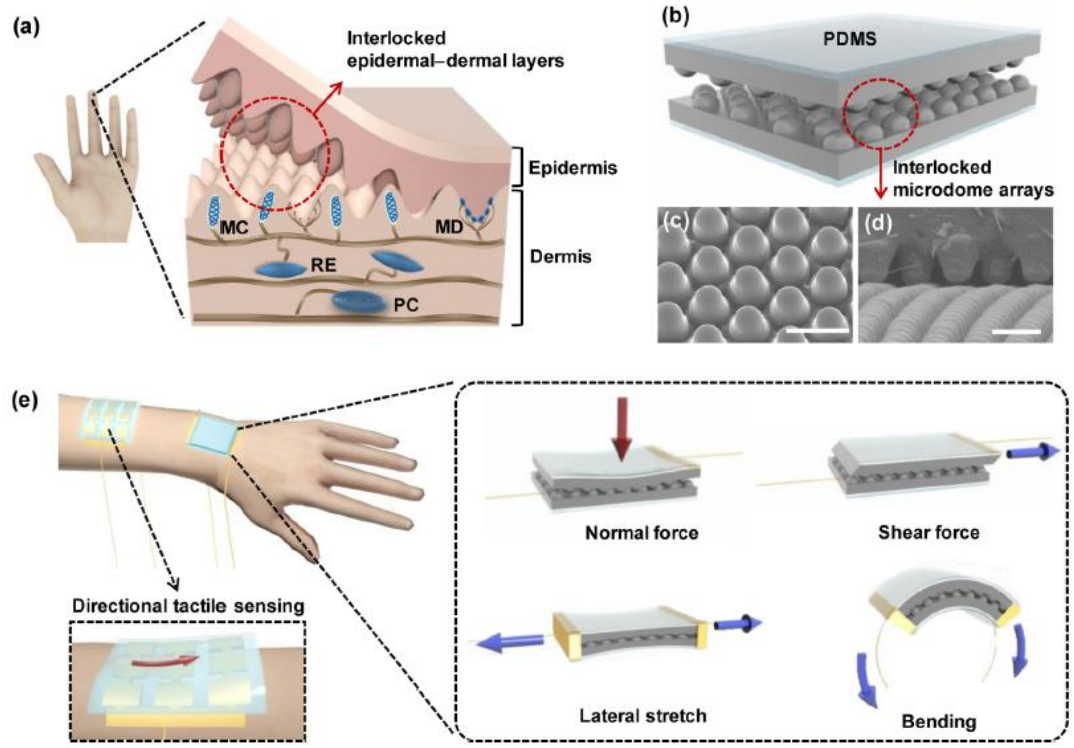

Figure 2.9 a) Overview of Fingertip's Epidermis and Dermis Layers. b), c), d) Micropillar Structure CNT/PDMS based Piezoresistive E-skin. e) E-skin which attached on Human Skin for various Forces Detection (Park et al., 2014b).

Furthermore, pyroelectric for temperature detection and piezoelectric approach with better dynamic sensing has been integrated with piezoresistive based micropillar structure e-skin in 2015 by similar group mentioned above. Overview of this design is showed in Figure 2.5 (Park et al., 2015). Shear pressure sensing was also improved by manipulating the degree of bending of micropillar using ion beam bombardment method. The results showed that shear force applied away from the direction of curvature shows increase in resistance and vice versa. This is due to contacted area of micropillars decrease when it shears away hence resistance increases. (Hasan et al., 2016).

2.5 Considerations in Fabrication Methods

Method or recipe which used to fabricate a device is important as this will affect the electrical properties or mechanical properties of the device. However, piezoresistivity behaviour of e-skin is more dependent on its electrical properties. Considerations and fabrication method for planar and microdomes/micropillars are discussed in this section.

According to the study on the behaviour of MWCNT in nanocomposites, electrical conductivity of this positive pressure coefficient material can be classified into three stages as shown in Figure 2.4 which related to the percolation behaviour. Several methods have been designed to fabricate tactile sensor with this behaviour such as coagulation, in-situ polymerization, melt-mixing compounding, oxidation and sonication. These methods are proposed to tackle the inherit problem in CNT which is aggregation of itself due to the van der Waals force of attraction and steric effect that noticed by few researchers (Bokobza, 2007, Alamusi et al., 2011). Hence, the formation of percolation pathway become harder based on the 3D numerical model. According to investigation of methods mentioned, curing temperature is one of the parameters dominates the dispersion of CNT in polymer and sensitivity of e-skin. Interesting fact also found that lightly aggregated CNT contribute in lowering percolation threshold (Alamusi et al., 2011).

Furthermore, optimization on dispersion of CNT in PDMS is done by disperse CNT into strong organic solvent, chloroform. An interesting empirical result shows that CNT and chloroform mixture would started to become optically non-transparent for concentration more than 0.3 $mgcm^{-3}$, hence agglomeration is not able to be observed easily using bare eyes (Liu and Choi, 2012). Although shear mixing helps to disperse CNT in PDMS more evenly, however it shortens CNT's length which affects the performance of sensor. So, sonication process is recommended to mix CNT in organic solvent within certain period of time depends on the frequency of agitation created by sonicator. Same effect also found in mechanical stirring that creates high shear force. Besides, magnetic stirring is essential in shortening the mixing time of the PDMS base polymer in organic solvent.

CHAPTER 3

METHODOLOGY

3.1 Overview

The overview of the project flow implementation is showed in Figure 3.1.

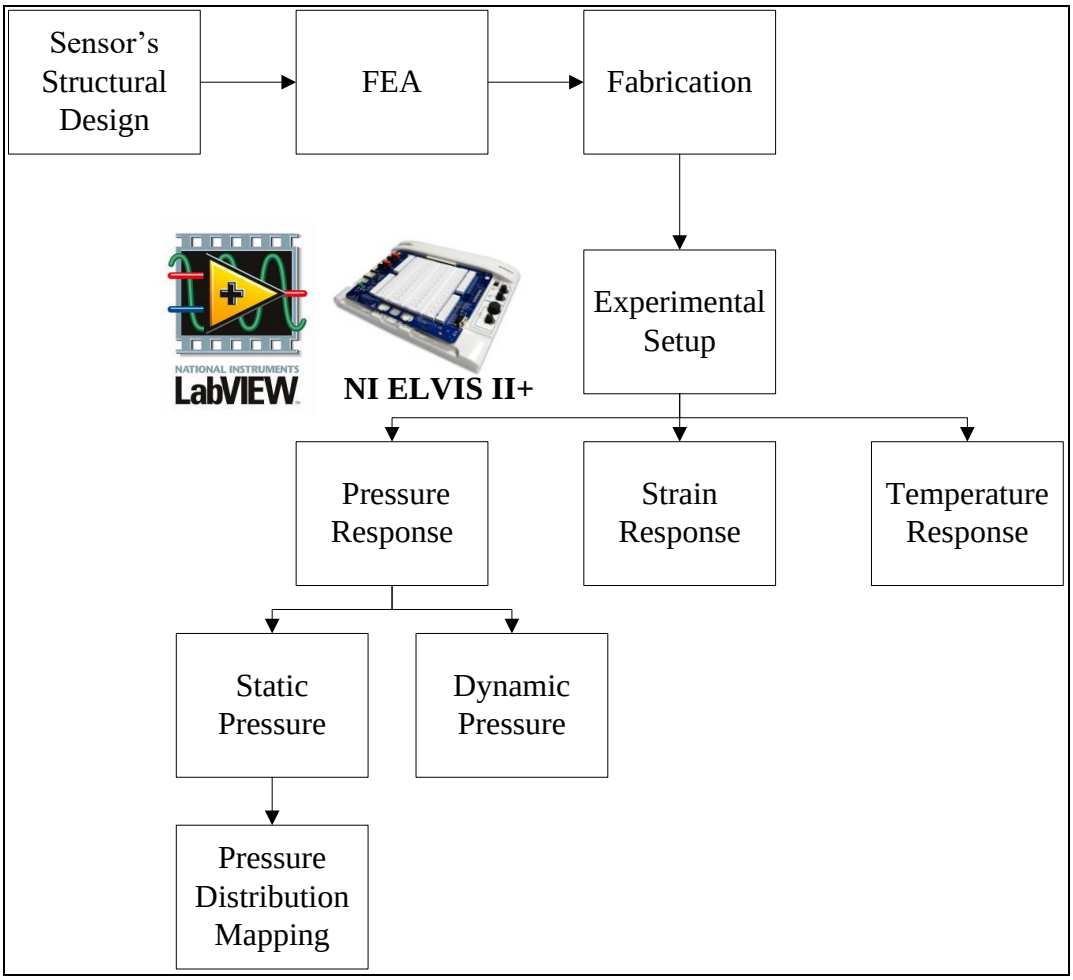

Figure 3.1 Schematic Illustration of the Project Flow

The project overview is depicted in Figure 3.1. Firstly, matrix structure e-skin with 3 × 2 square pads and the serpentine structure e-skin were designed. After that, Finite Element Analysis (FEA) was done to investigate the mechanical deformation of e-skin structure under tensile strain and applied pressure. Next, A PDMS mold was prepared based on the structural design of the sensor. Besides, the method of e-skin fabrication which showed in Section 3.4 was identified from the literature review and some changes were done with a few different considerations which have been stated in Section 2.5. Finally, parameters of e-skin including temperature sensitivity, tactile sensitivity for both static and dynamic force, stretchability and pressure distribution across the sensor under static pressure were characterized through some experiments.

3.2 Structural Design and Finite Element Analysis (COMSOL Multiphysics)

3.2.1 Introduction

Finite Element Analysis (FEA) is a computational analysis used in solving boundary value problems using numerical method (Hutton, 2004). Normally, a physical behaviour of an object can be modelled mathematically as a differential equation and solved based on the boundary conditions imposed. The physical changes of the object under different physical conditions can be predicted from the approximate solution with good accuracy. This analysis is started by parameters setting including the material properties, the geometric properties and type of finite elements known as preprocessing. The finite elements can be either in quadrilateral or triangle which is different in term of degree of freedom. After that, the solution is obtained in term of field variables of the analysis based on the boundary condition defined. The finite element solution which obtained is plotted in a graph or shape changes in the original drawing. In this work, COMSOL Multiphysics 3.5, a mathematical modelling software was used to undergo FEA, which designed for solving scientific and engineering problems (Andersw, 2008).

The 3D structural design of e-skin was drawn using COMSOL, as showed in Figure 3.2. After that, the deformation of e-skin's mechanical structure was analysed using structural mechanics module in COMSOL. To simplify the analysis, 2D cross section of the single element's structure with different sizes were drawn to compare the effect of structural deformation and pressure distribution.

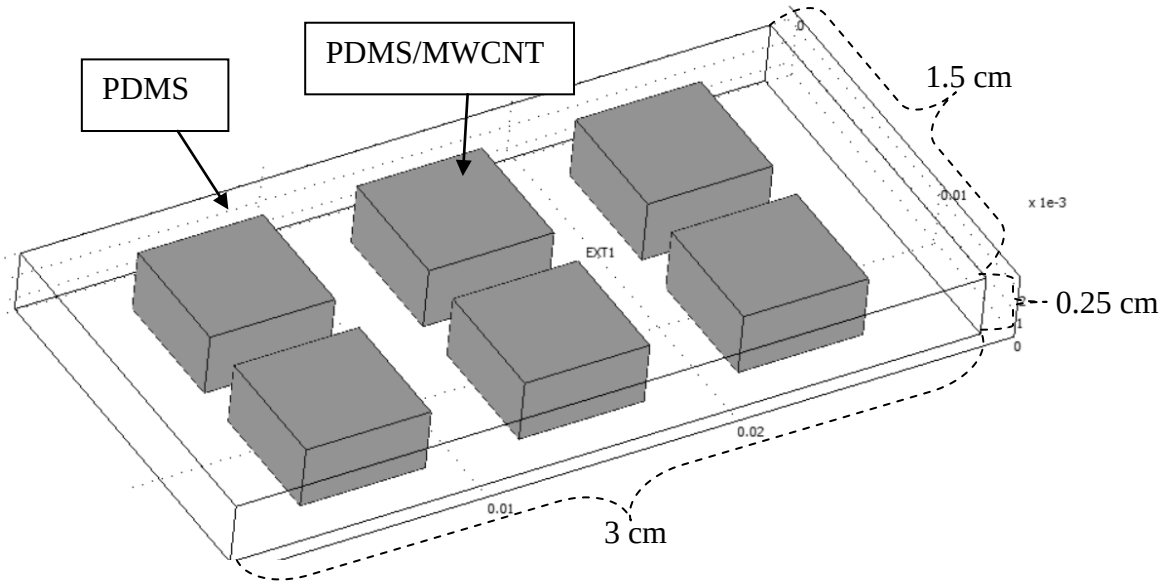

Figure 3.2 Matrix Structure of E-skin

3.2.2 Parameter Settings

Material parameters used in the simulation are Young's modulus, *E*, 7.5 x 10^5 Pa, Poisson's ratio, *v*, 0.49 and density, ρ of 965 kgm^{-3} (Mark, 1999). Geometrical sensor model is depicted in Figure 3.2 with the dimension of, 1.5 cm × 3 cm × 0.25 cm. A boundary load pressure of 60.5 kPa (this value is set according to the largest normal force applied in FEA, done by Park et. al. (Park et al., 2014a)) was exerted at the upper part of the sensor with a fixed movement at the bottom layer.

3.2.3 Serpentine Structure (Optimize in Strain Performance)

By referring to Figure 3.2, the matrix structure shown was optimized for tactile sensing, whereas in Figure 3.3, the serpentine structure was optimized for strain sensing (Lu et al., 2012). This spring-like structure which designed by John Rogers et al. has been proved in enhancement of stretchability of the e-skin (Zhang et al., 2014, Zhang et al., 2013). The dimension of the square pad in serpentine is 5 mm × 5 mm, inter-distance between square pads is 1 cm and total length is 3.5 cm. The width of the spring shape is 1mm which is the smallest dimension capable by the photolithography machine. Besides, the spring shape was designed by linking an upper semi-circle and another lower semi-circle. It is known as a one unit cell according to the structure which defined by John Rogers et al. (Zhang et al., 2013).

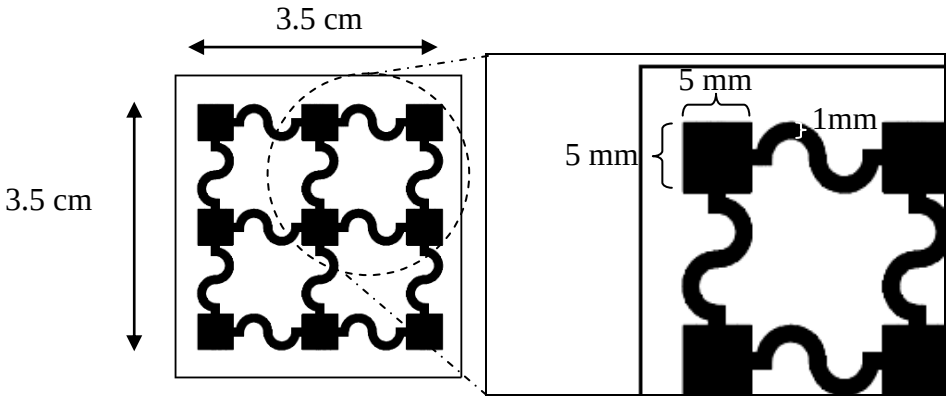

Figure 3.3 Serpentine Structure of E-skin (Mask for Serpentine Mold)

3.3 Fabrication Process

3.3.1 Equipment

The equipment which was used in the fabrication process are beaker, disposable Petri dish, hot plate, sonicator, vacuum desiccator, vortex mixer and weight balancer.

3.3.2 Materials

Materials that involve in e-skin fabrication are copper electrode, chloroform, hexane, MWCNT, Slygard® 184 Silicon Elastomer (PDMS base with curing agent), PDMS mold with silicon wafer (matrix structure mold) and photoresist with PCB (serpentine mold).

Chloroform is a strong organic solvent which used to disperse MWCNT evenly into PDMS base solution. It was chosen based on its dispersion behaviour as compared to other organic solvents including chloroform, toluene, tetrahydrofuran (THF) and dimethylformamide (DMF) (Liu and Choi, 2012). One of the comparisons is the stability of composite solution after sonication by pre-dissolution of PDMS base into the organic solvents and mixed with MWCNT later or conversely were determined. According to their findings, dispersion of MWCNT in the composite solution with chloroform was visually stable after sonication for 42 hours. However, two layers of separated solution were observed in MWCNT/PDMS composite for the remaining solvents due to the instability in dispersion within 20 hours. Hence, the result of the experiment shows that the chloroform is the most suitable organic solvent to dissolve MWCNT and PDMS base.

MWCNT, which involve in the fabrication was obtained from Chengdu Organic Chemicals Co. Ltd. It has outer diameter of less than 8nm, length ranging from 10 – 30 (μm), purity more than 95 weight% and electrical conductivity of more than 100 Scm^{-1}. Soft elastomer, Slygard® 184 Silicon Elastomer used is a PDMS elastomer kit which purchased from Dow Corning Corporation. It is suitable for stretchable sensor application especially in e-skin sensor due to its biocompatibility and hemocompatibility (Livermore, 2004).

In order to fabricate a serpentine shape e-skin, the mold was created using PCB printing technology. The PCB was laminated with 4-layer of photoresists to create certain layer of thickness for the MWCNT/PDMS. The fabrication procedure for serpentine mold is shown in next section.

3.3.3 Procedure

3.3.3.1 Mould Fabrication (Using PCB Printing Technology)

The procedure to fabricate a serpentine structure mold was fabricated using PCB printing technology is listed as below:

1. A predesign mold was printed out on a tracing paper as the mask.
2. A layer of dry film photoresist was laminated on the PCB.
3. Photolithography technique was used to create the mold by cover the serpentine mask on the PCB and exposed to ultraviolet (UV) light for 12 seconds.
4. Another layer of photoresist was laminated to the UV exposed photoresist on PCB and repeat step 3 until 4 layer of photoresists were laminated.
5. The UV exposed photoresist was soaked in developing solution for 1 hour and serpentine structure mold is obtained.

3.3.3.2 E-skin Fabrication

The procedure of the e-skin fabrication (matrix structure & serpentine) is listed as below and visualized in Figure 3.5:

1. MWCNT (0.32 g) mixed with chloroform (80 ml) which was extracted out using micropipette in the concentration of 4 mg/cm^3.
2. The mixture solution was sonicated for 1 hour to separate the agglomerates of MWCNT.
3. PDMS resin (3.68 g) was extracted out using micropipette and mixed with the chloroform solution (10.5 ml) using magnetic stirring in 1150 rpm for 15 minutes to yield a less viscous solution.
4. Both solutions were mixed manually to yield an 8 weight % MWCNT/PDMS composite and went through additional sonication for 2 hours.
5. The MWCNT/PDMS mixture was heated at 62˚C in the vacuum oven until the chloroform was completely vaporised in 1 hour. This can be observed

from the decrease in volume of the MWCNT/PDMS solution contained in the beaker and it appears in viscous form.

6. Before the MWCNT/PDMS mixture casted on the mold (applicable for serpentine structure only), MWCNT/PDMS composite was mixed with mixture of hexane and PDMS curing agent (PDMS curing agent is mixed with PDMS in the ratio of 1:10.) in the density of 0.5 gcm^{-3}.
7. It was put inside a vacuum oven to remove the trapped hexane and bubbles before thermal curing at 80˚C for 15 minutes to yield a viscous MWCNT/PDMS composite.
8. The MWCNT/PDMS composite was casted into the square pad location in the PDMS mold with conducting side of flexible copper electrode placed on the silicon wafer as the base.
9. Another copper electrode is placed on top of square pad location for tactile sensing capability which is visualised in the bottom of Figure 3.5.
10. The MWCNT/PDMS composite with PDMS mold was put into the vacuum oven for 2 hour thermal curing. If curing is done in room temperature it might create MWCNT agglomeration which eventually affect its electrical conductivity was shown in Figure 3.4.

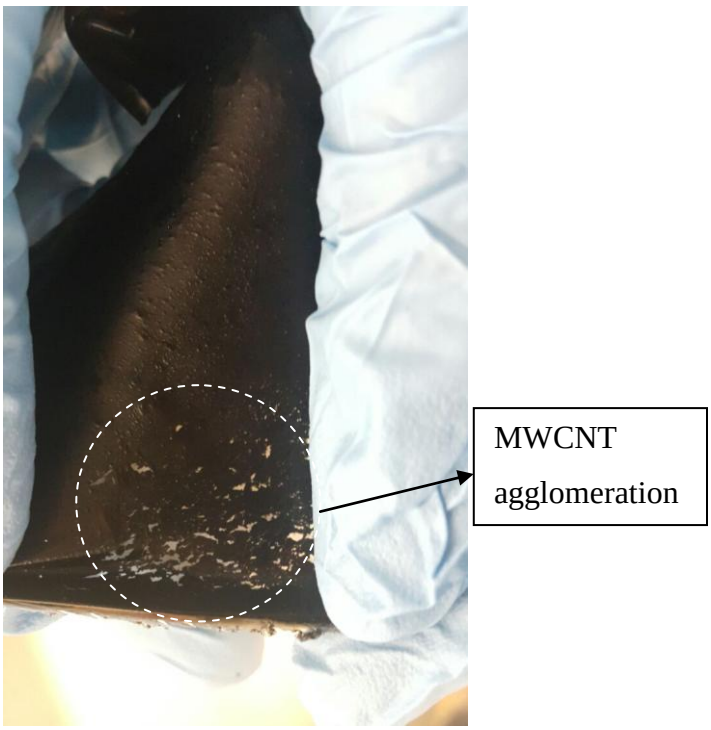

Figure 3.4 MWCNT/PDMS composite cured overnight

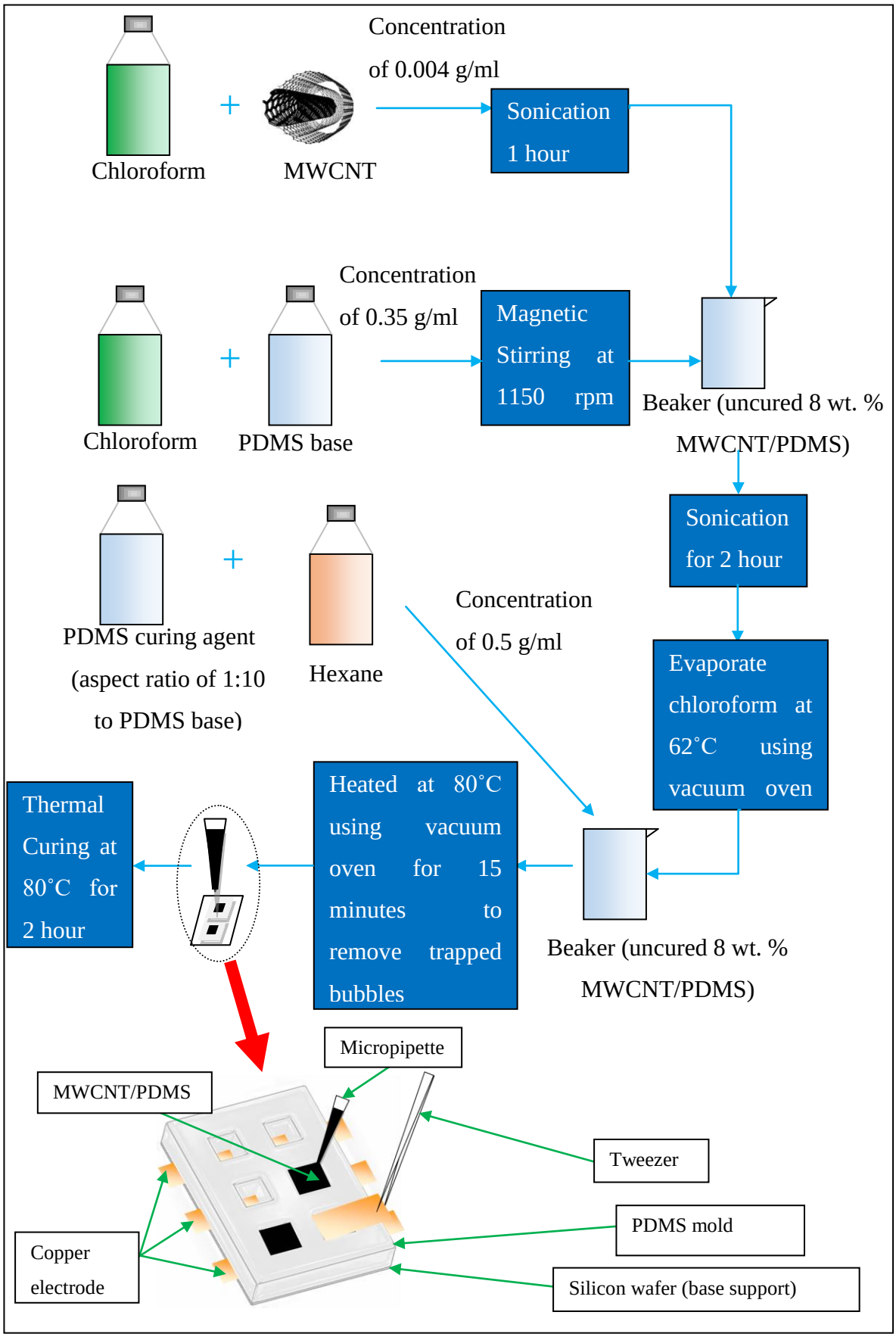

Figure 3.5 Fabrication Method Overview (Matrix Structure only)

3.4 NI ELVIS II+ and NI LabVIEW

In this project, resistance measurement is the parameter which needed to be characterized corresponding to other manipulating variables. The piezoresistance of the e-skin is more than 1 MΩ, and hence it is not able be measured using a normal multimeter (Park et al., 2014a). Normally, a source measuring unit (SMU) or high-end digital multimeter (DMM) is used to measure the piezoresistance. Due to the availability of measuring instruments, NI ELVIS II+, a modular engineering educational laboratory platform from National Instruments has offered measurement and data-logging. DMM of this module has offered a high resolution, 5.5 digit measurement, and resistance measurement up to 100 MΩ. The connection of device under test (DUT) is showed in Figure 3.6 as Rx, whereas R_{LEAD} from the test lead is negligible. To obtain more accurate measurement, software compensation by nulling the R_{LEAD} is done.

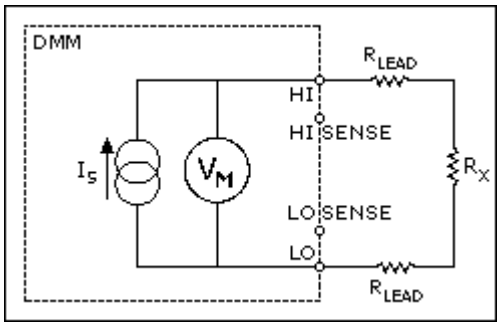

Figure 3.6 Resistance Measurement using DMM (Anon., 2016)

NI LabVIEW is a visual programming language which ease the users in programming using data block which execute code in parallel rather than sequential text code such as C, C++ or Python (Instruments, 2012). It is commonly used in data acquisition and analysis, automated testing, instrument control or embedded control and monitoring system. Hence, it is used along with NI ELVIS II+ to acquire data for characterization of e-skin sensor in this project. By utilising this platform, mathematical operation on the data collected can be done easily by programming in the block diagram and it also able to output the collected data into excel. The LabVIEW Virtual Instrument (VI) which used to measure the piezoresistance is shown in Figure 3.7.

Firstly, the subVI in step 1 was configured as 2-wire measurement and the resistance is configured from 0 to 100 MΩ. An internal current source of 500 nA was chosen according to the specification sheet of NI ELVIS II+ showed in Figure 3.8. Next, a DAQmx start block is inserted to run the program when start button is pressed. The grey square box which shown in step 3 is a while loop with 1000 ms delay per loop and the one sample is taken per loop for one channel. The loop is terminated when the stop button is pressed or error occurs in the configuration every execution. If the time taken is longer than 100 s, the data showed in the scope will be cleared off and restart. The scope block chosen is waveform graph which output double data type in with increment with time. After that, step 4 reset the Task when the loop in step 3 is terminated and output if there is any error message in step 5.

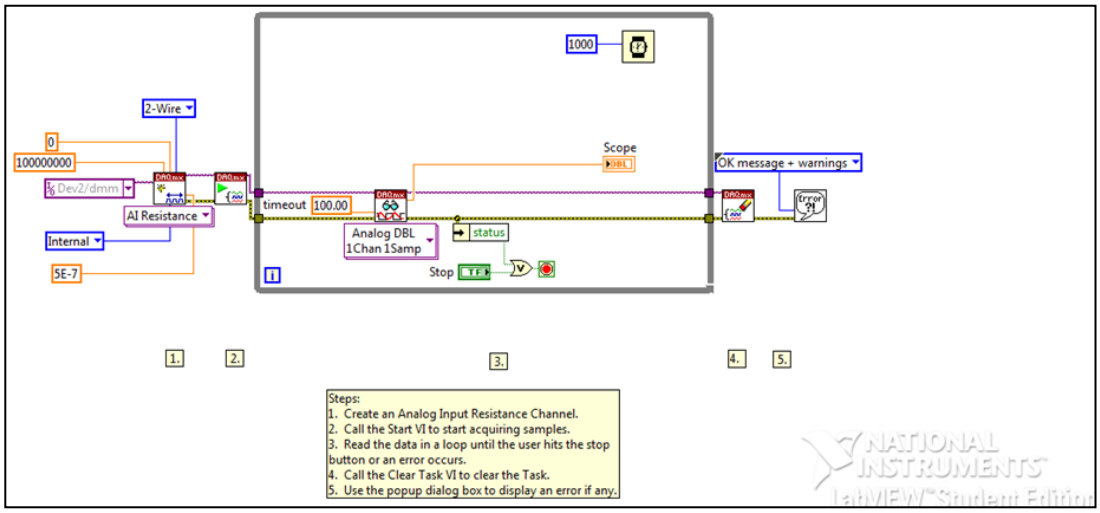

Figure 3.7 Block Diagram Panel of LabVIEW VI

Resistance Measurement Accuracy ±(ppm of Reading + ppm of Range)

Range	Test Current	Max Test Voltage	1 Year (Tcal ±5 °C)	Tempco/°C (15 to 35 °C)
100 Ω	1 mA	100 mV	450 + 310	70 + 55
1 kΩ	1 mA	1 V	450 + 100	70 + 12
10 kΩ	100 µA	1 V	450 + 100	70 + 12
100 kΩ	10 µA	1 V	450 + 100	70 + 12
1 MΩ	5 µA	5 V	450 + 100	70 + 8
100 MΩ	500 nA	5 V	8000 + 75	400 + 4

Figure 3.8 NI ELVIS II+ DMM Resistance Measurement (Communications, 2009)

3.5 Experimental Setup of Characterization

3.5.1 Static Pressure Response

Static Pressure Response was used to test the tactile sensitivity of the e-skin towards the external static pressure. The fabricated e-skin sensor was connected to a pair of DMM probe and finger was used to exert pressure on the square pad area. Intensity mapping was performed to show the pressure distribution within the square pad. The experimental setup is shown in Figure 3.9.

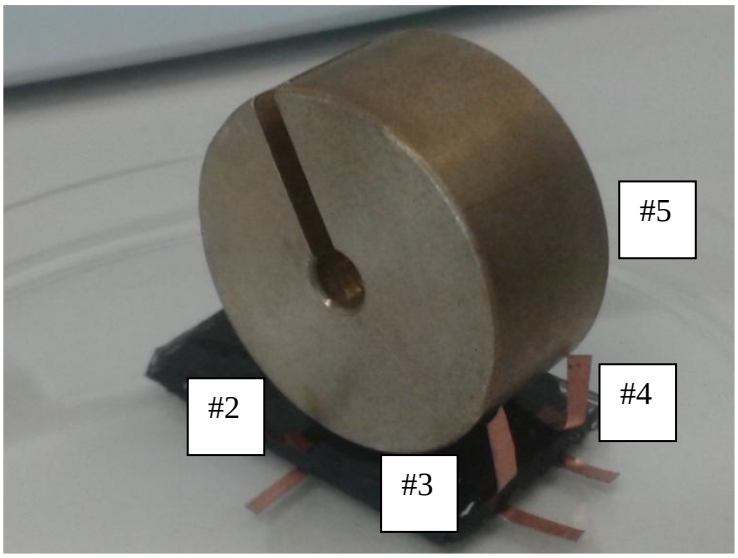

Figure 3.9 Setup of Intensity Mapping

3.5.2 Dynamic Pressure Response

Dynamic Pressure Response was used to test the tactile sensitivity of the e-skin towards the external dynamic pressure. It was characterized by rolling a Malaysia Ringgit 20 cent coin on one of the column. The setup is shown in Figure 3.10.

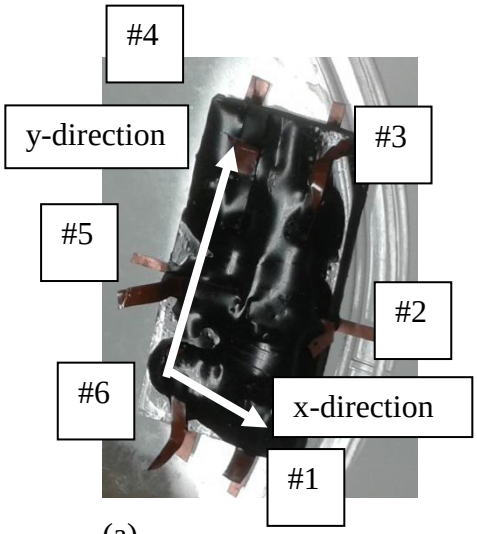

(a)

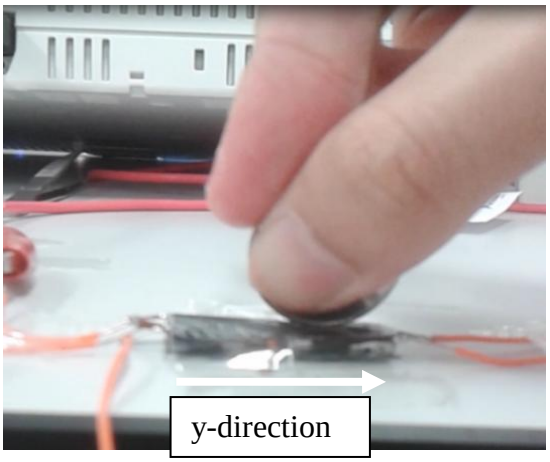

(b)

(c)

Figure 3.10 (a) Top View of E-skin (b) Setup of Dynamic Pressure Response (Side View of E-skin) (c) Malaysia Ringgit 20 cent

3.5.3 Strain Response

The strain capability of the sensor is somehow limited due to the thickness of e-skin prototype, hence stretching of the sensor is done by using hand as showed in Figure 3.11.

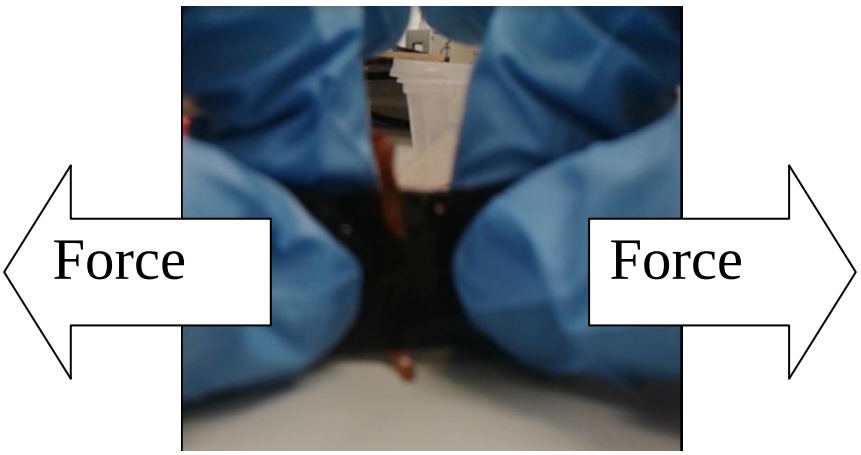

Figure 3.11 Stretching E-skin Using Hand

3.5.4 Temperature Response

Hot and cold sensation which able to be detected by us shows that our skin is sensitive towards the change of temperature. This fabricated sensor was further tested on its sensitivity towards temperature variation. The temperature induced on the skin was controlled using a hotplate with temperature ranges from 27 ˚C to 60 ˚C (Karimov et al., 2011, Morteza et al., 2015). The temperature indicated in the display of the hotplate was verified using an infrared thermometer. Resistance change of the e-skin was measured using DMM with the setup depicted in Figure 3.12.

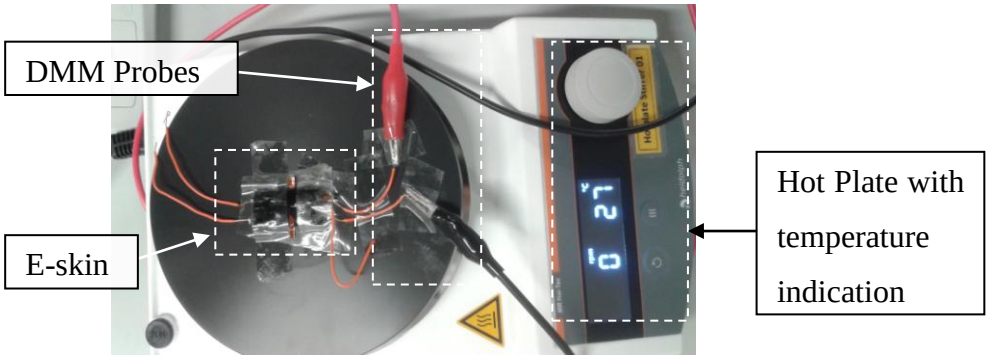

Figure 3.12 Temperature Response Experimental Setup

CHAPTER 4

RESULTS AND DISCUSSION

4.1 Overview of Characterization

In this chapter, the yield strength test of the planar structure e-skin was performed using Instron 5848. Besides, results of FEA analysis for e-skin structures such as the matrix structure and serpentine structure under mechanical deformation were analysed. After that, the characteristics of e-skin parameters: dynamic and static pressure, temperature and strain were shown. Lastly, Scanning Electron Microscope (SEM) was used to observe the surface and cross-sectional structure of the e-skin.

4.2 Yield Strength of Planar E-skin

The stretchability of the developed device was tested using Instron 5848 microtester machine. A test specimen with rectangular planar structure MWCNT/PDMS composite has the dimension of 4 cm × 1 cm × 0.045 cm (length, width and height) was used. This machine is suitable to be used in characterizing the stretchability of the material because it is able to provide nanometre strain movement (ShilalLa, 2006). The experimental setup and result of the yield strength test are showed in Figure 4.1 and Figure 4.2, respectively. The yield strength for this specimen is 5.5013 $kgfcm^{-2}$. The MWCNT/PDMS speciment is able to be elongated for 53.75% of its original length where 21.5 mm of extension is the fracture point of the specimen (Liu, 2011).

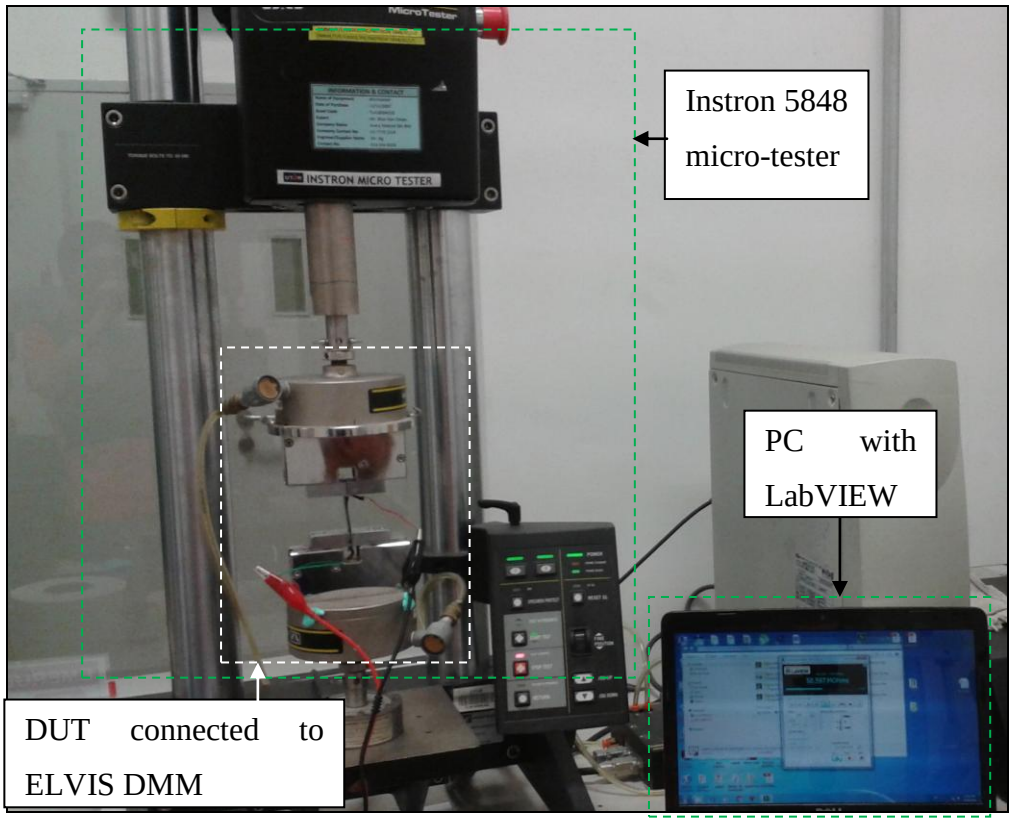

Figure 4.1 Experimental Setup for Strain Response Test

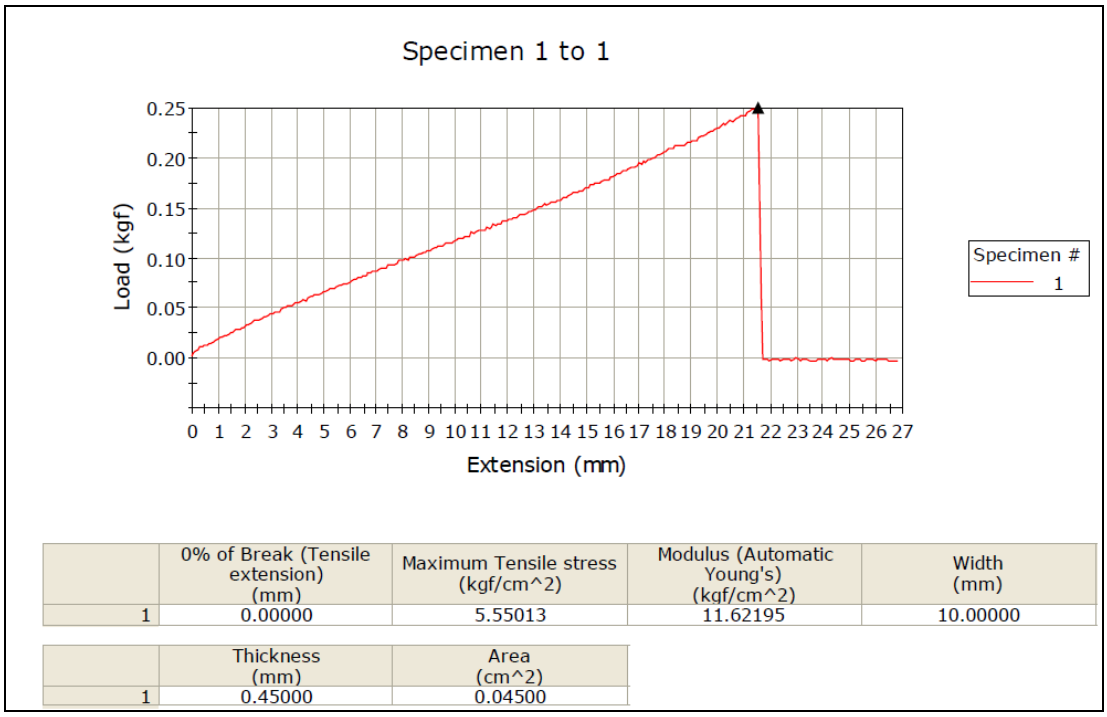

	0% of Break (Tensile extension) (mm)	Maximum Tensile stress (kgf/cm^2)	Modulus (Automatic Young's) (kgf/cm^2)	Width (mm)
1	0.00000	5.55013	11.62195	10.00000

	Thickness (mm)	Area (cm^2)
1	0.45000	0.04500

Figure 4.2 Yield Strength Test Result using Instron Machine

4.3 FEA Results

4.3.1 Matrix Structure

The 2D cross-section from top view of the e-skin was analysed for its von Mises stress distribution and total displacement change. It is a quantitative result which shows the effective stress distribution of the external pressure on the e-skin structure. FEA was carried using the parameters mentioned in Section 3.2.2. The simulation parameters for 8 weight% of PDMS/MWCNT are different from pure PDMS hence the simulation is just an approximation on its behaviour.

The total displacement change of the e-skin has shown in Figure 4.3(a) increases gradually from the middle to both ends. It is noted in Figure 4.3(b), the stress is focused in middle of the e-skin and gradually decreased to the both ends. The colour intensity bar showes a constant pressure of 52.4 kPa distributed across the e-skin structure.

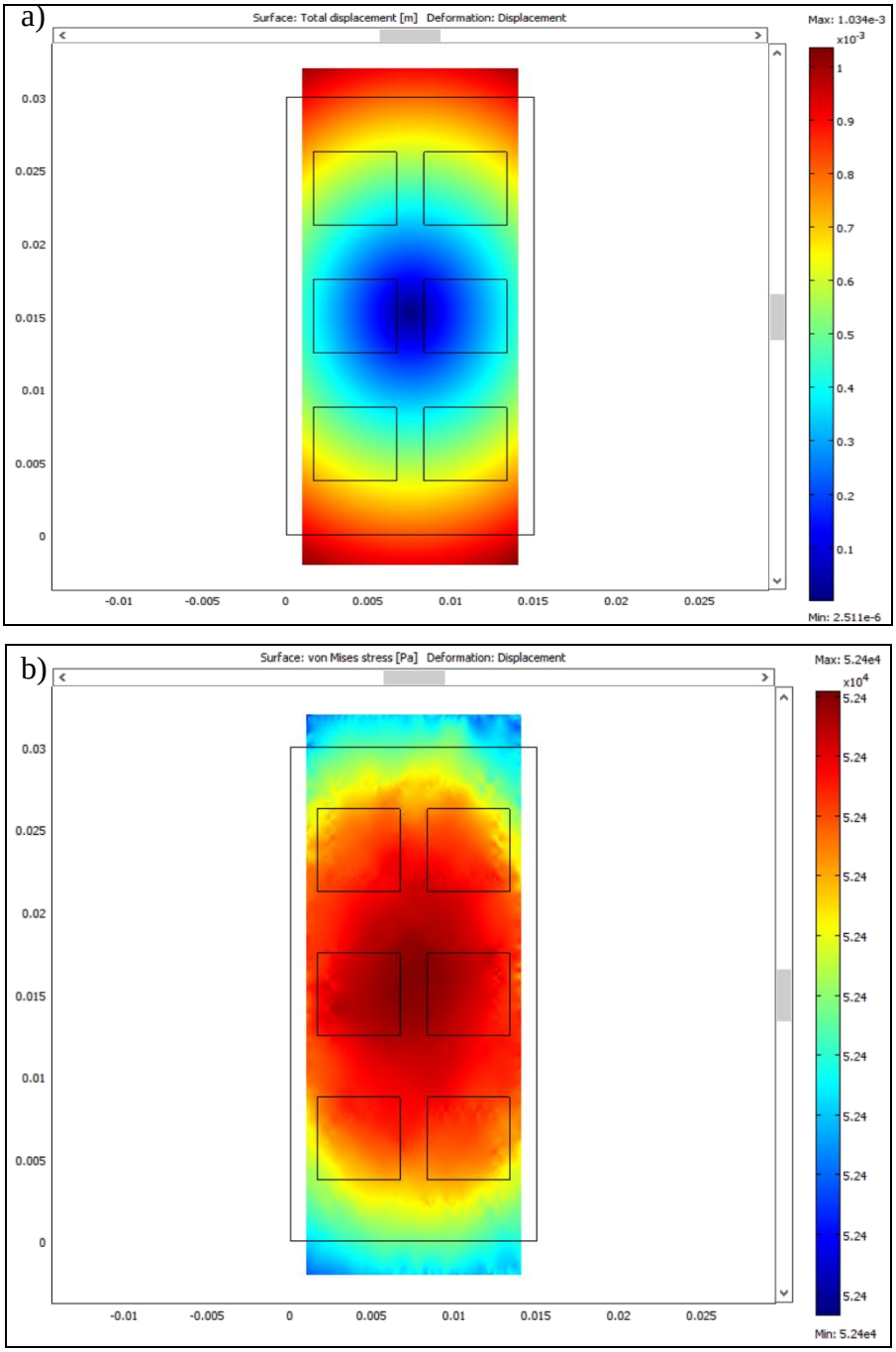

Figure 4.3 FEA of Matrix Structure E-skin under Strain Stress (Top View) (a) Total Displacement Change (b) Von Mises Stress Distribution

By applying a normal pressure of 60.5 kPa from top, von Mises stress distribution across the e-skin model is shown in Figure 4.4. It was investigated by fixing the movement at the bottom of e-skin. From Figure 4.4, it can be observed that the pressure exerted on the square pad is transferred to the bottom's corner of the e-skin.

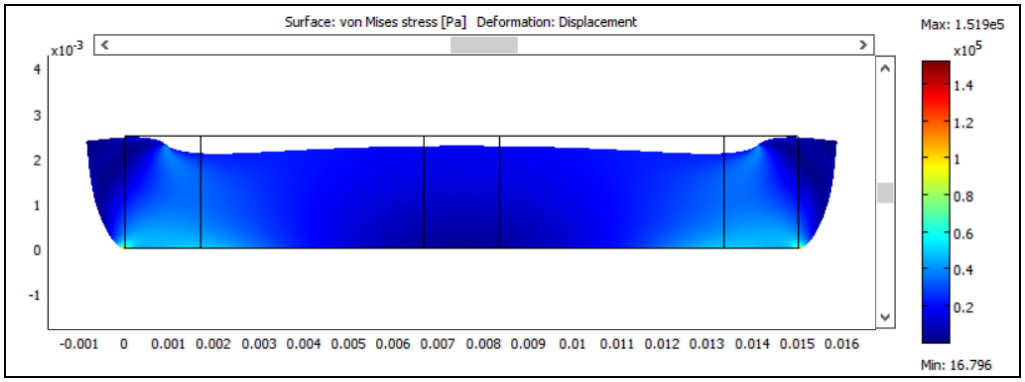

Figure 4.4 FEA of Matrix Structure E-skin under Normal Force Compression

4.3.2 Serpentine Structure

The serpentine structure of single unit cell was simulated for several geometrical parameters including the thickness, location of the spring shaped interconnection and size of the square pad. By referring to Figure 4.5, the third structure counting from top shows a greater change in its displacement compares to the remaining design and hence, in this project the structure was chosen for e-skin design. The dimension of this structure is shown in Figure 3.3.

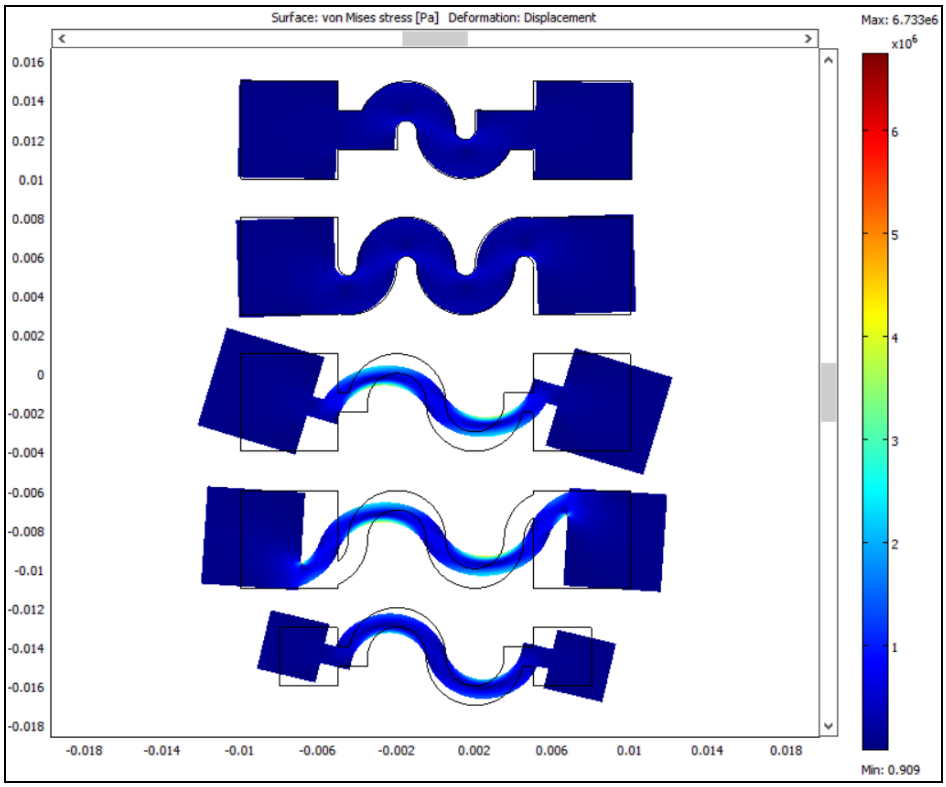

Figure 4.5 FEA of Serpentine Structure E-skin

4.4 Device Fabrication

4.4.1 Matrix Structure Prototype

Figure 4.6 shows a successfully fabricated matrix structure device with the embedded copper electrode. Uneven structure in the MWCNT/PDMS was observed. This might due to the squeezing of MWCNT/PDMS during the placement of the copper electrodes from the respective location and mix with the neighbour copper pin.

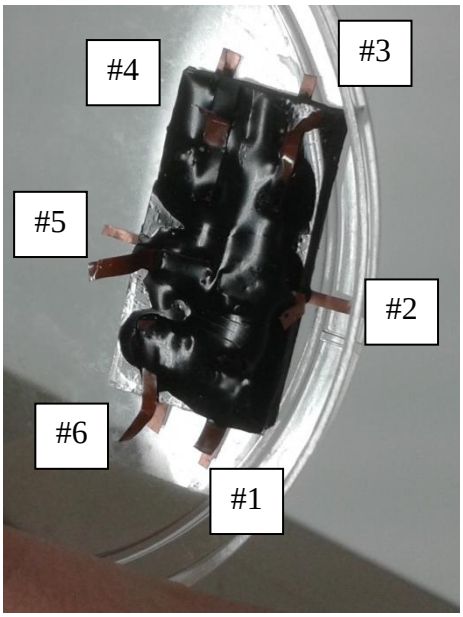

Figure 4.6 Fabricated Matrix Structure E-skin

4.4.1.1 Scanning Electron Microscope (SEM) Result

SEM was used to observe the surface of e-skin and the agglomeration of MWCNT in the MWCNT/PDMS composite. The cross-sectional view of the e-skin was captured and showed in Figure 4.7 and 4.8. Besides, the e-skin with the irregular surface was captured and showed in Figure 4.9 and 4.10.

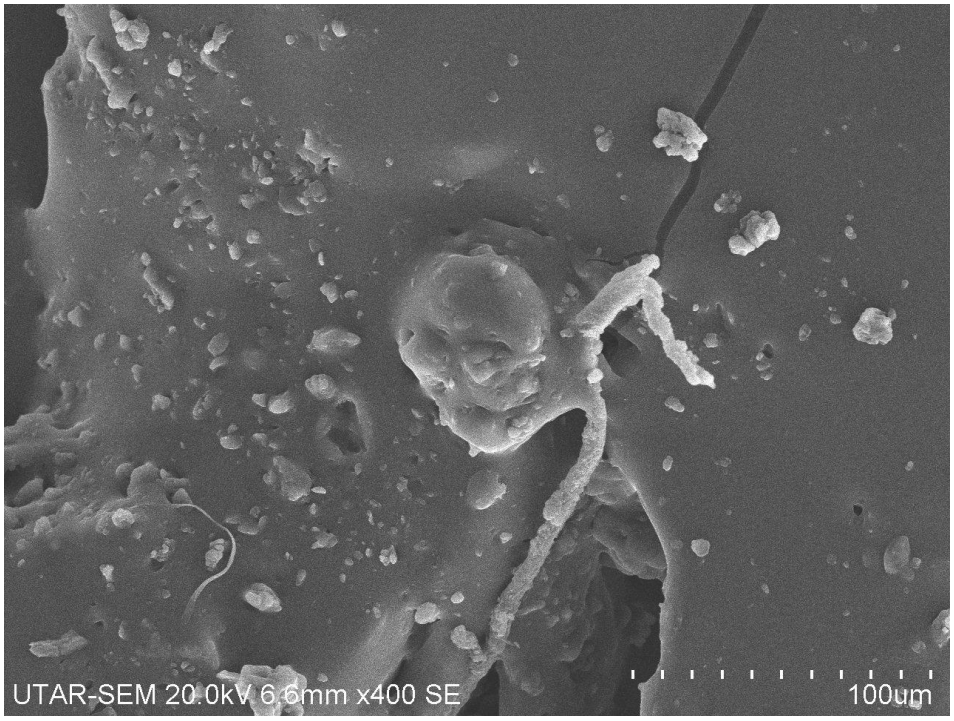

Figure 4.7 SEM Image on the Cross-section of E-skin (× 400 magnification)

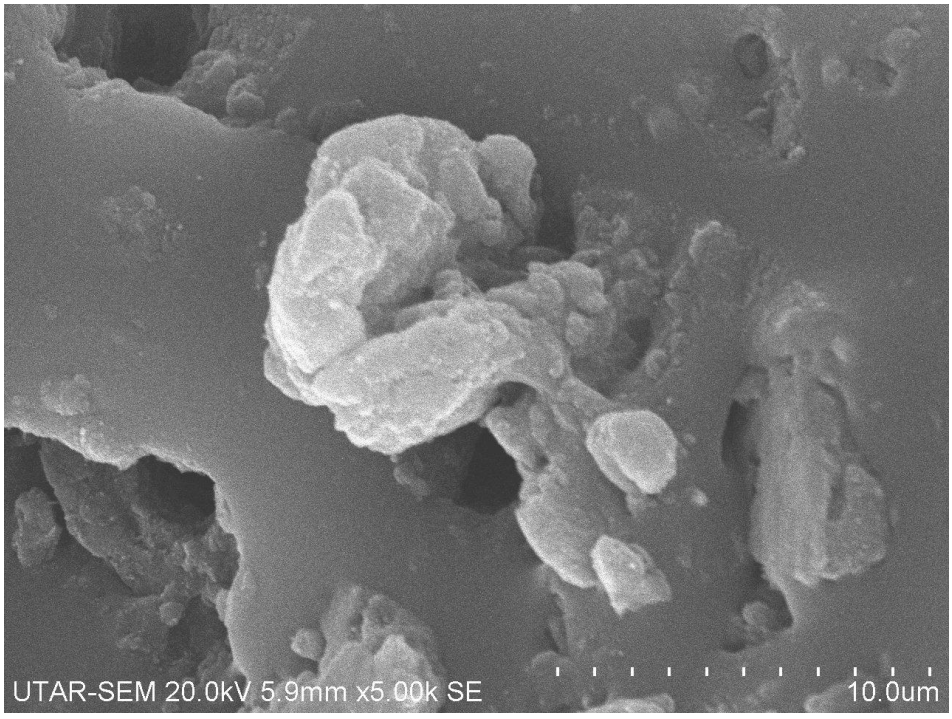

Figure 4.8 SEM Image on the Cross-section of E-skin (× 5000 magnification)

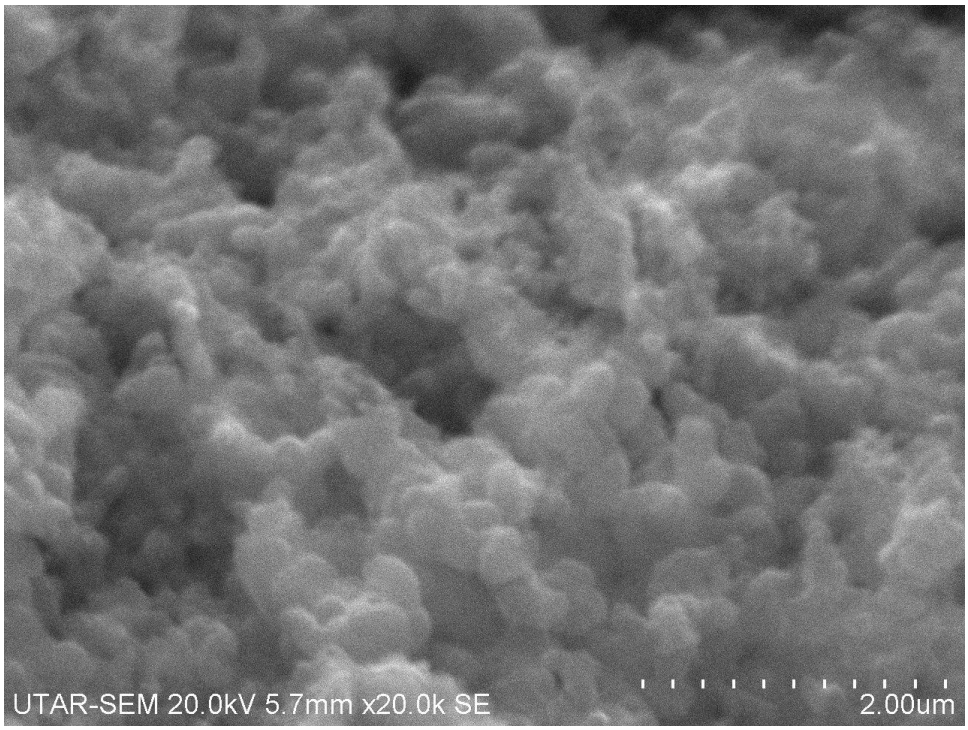

Figure 4.9 SEM Image on the Surface of E-skin (× 20000 magnification)

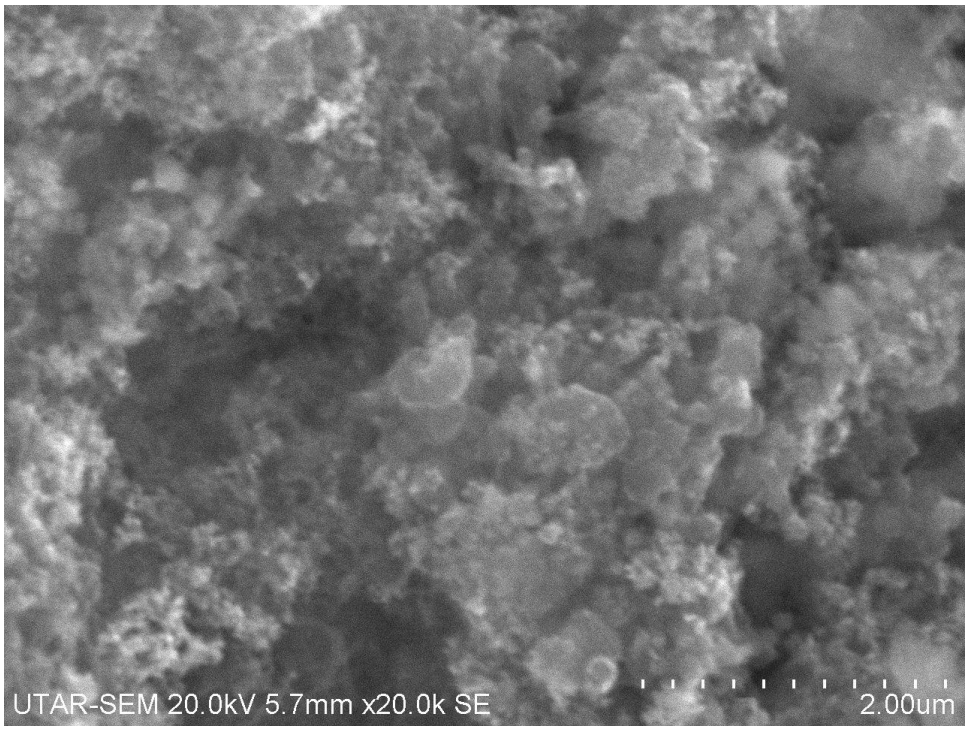

Figure 4.10 SEM Image on the Surface of E-skin (× 20000 magnification)

4.4.2 Serpentine Structure Prototype

The fabricated serpentine experiences structure rupture in the de-moulding process. One of the possible reason might due to the absent of antistiction, trichloro(1H,1H,2H,2H-perfluorooctyl)silane (FOTS) (Hasan et al., 2016, Zhang et al., 2010). Tweezer was failed to remove the MWCNT/PDMS composite from the mold after immersed them into isopropanol. So, the photoresist stripping solution was used to wash away the photoresist, but the serpentine structure has been broken due to strong adhesion on the PCB mold.

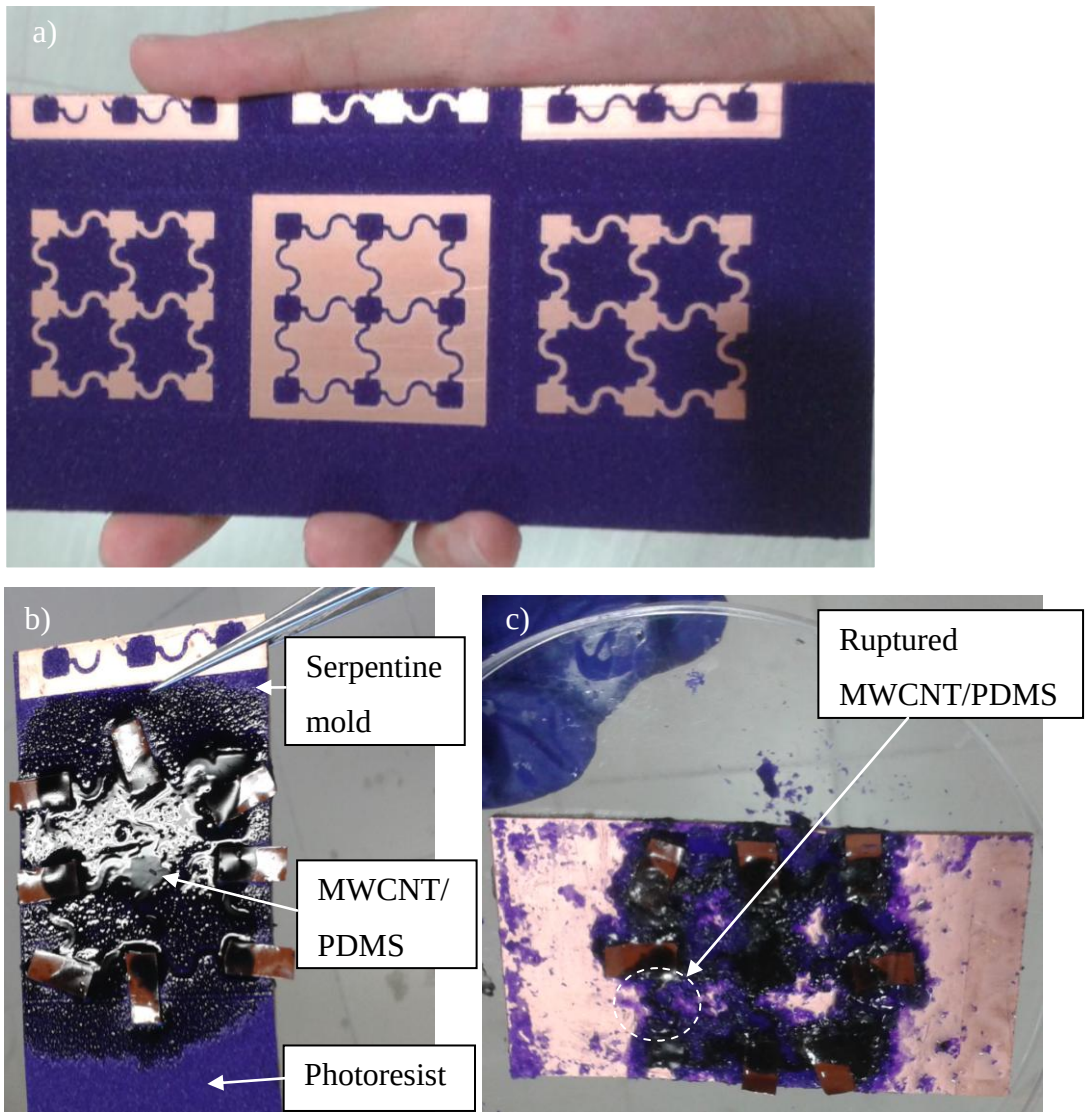

Figure 4.11 a) Serpentine Mold. b) Serpentine Structure E-skin (After Thermal Cured). c) Serpentine Structure E-skin (After Photoresist Etched Away).

4.5 Pressure Response

4.5.1 Dynamic Pressure Response

The dynamic response of the e-skin towards the shear force is showed in Figure 4.12 and 4.13.

The coin movement from pin #6 to pin #1, as depicts in Figure 4.12, shows a trough shape in the resistance change. This might due to the small inter-spacing between the PDMS/CNT. A large resistance changes was observed when the pressure is exerted on the respective square pad where most of the PDMS/CNT located. Similar response is noted when the coin is rolled in the reverse direction (from pin #1 to pin #6).

In Figure 4.13, the coin movement from pin #4 to pin #6 shows a similar trend in vertical direction, however a very clear trough shape is unobvious as there should be two inter-spacing between these pin. It might due to the movement of coin rolling is affected by the uneven surface of e-skin so the reduction of resistance at inter-spacing doesn’t reduce effectively. The resistance of the e-skin is increased due to the coin has squeezed the MWCNT in MWCNT/PDMS network apart and hence, the overall resistance increase.

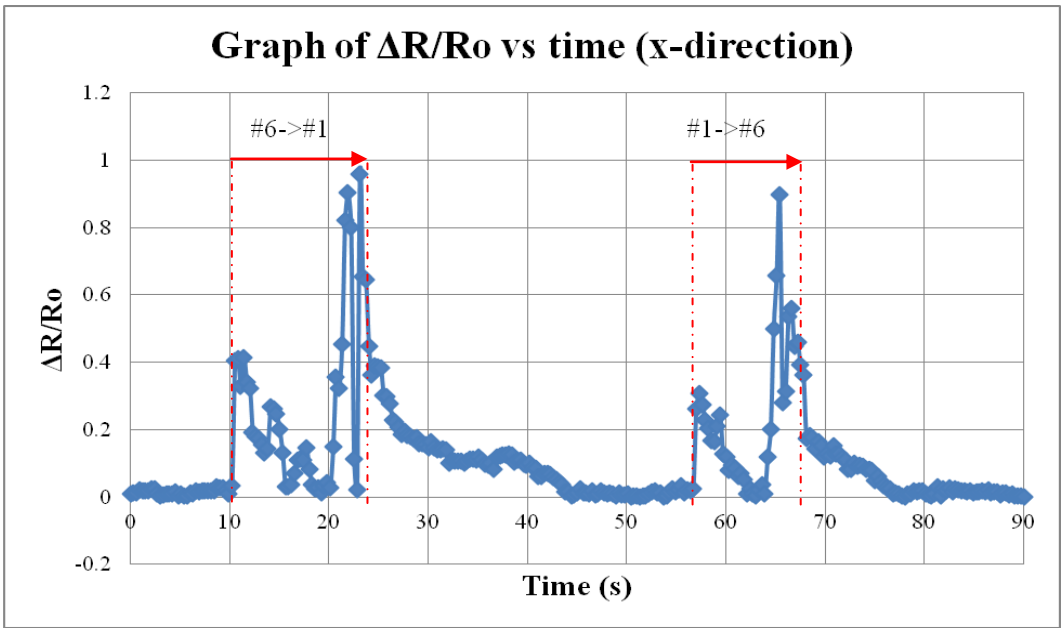

Figure 4.12 Dynamic Response of E-skin under X-direction Movement

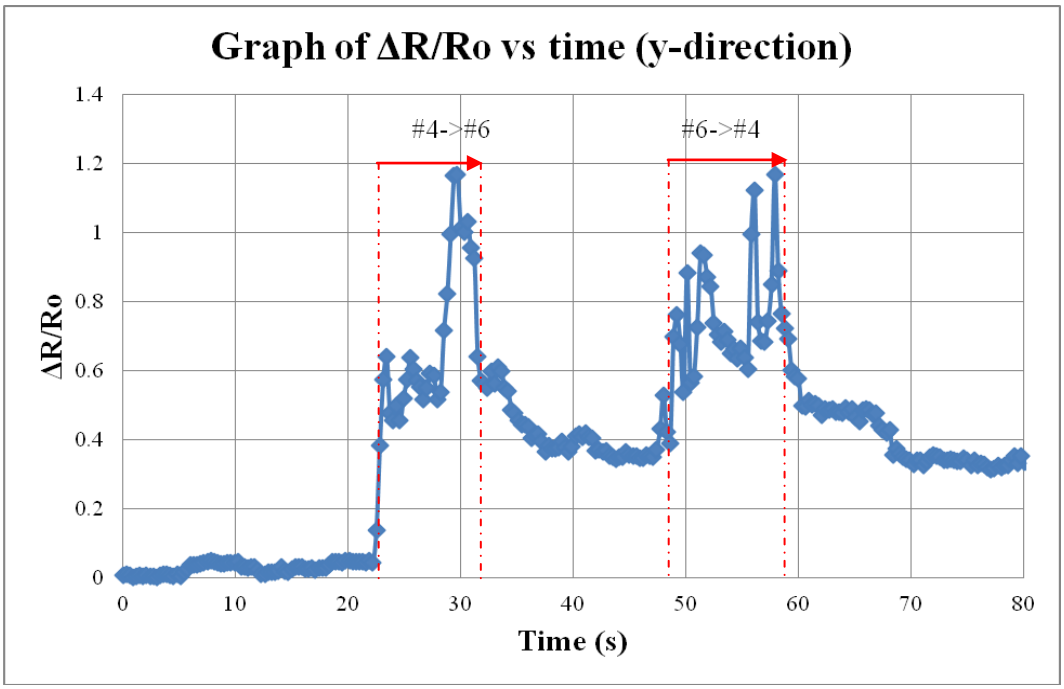

Figure 4.13 Dynamic Response of E-skin under Y-direction Movement

4.5.2 Static Pressure Response

The static pressure response of the e-skin was determined for the sensitivity of the resistance change towards the external static force directly on the square pad showed in Figure 4.14. A significant transient behaviour in the resistance change was observed and it showed overshoot in resistance when external pressure was removed which attributed to the viscoelasticity behaviour of the PDMS. It was proven in simulation by modelling the e-skin as in mechanical spring with damper and RC electrical circuit (Morteza et al., 2015, Firouzeh et al., 2015). The result illustrates a decrease in resistance when it was compressed by a static load. This is because the MWCNT network in the PDMS has becomes compact. When the MWCNTs in the percolating pathway become closer to each other, it shows a better conductivity. In addition, resistance shift is observed in Figure 4.13 and 4.14 after each sensing cycle. It is inevitable due to viscoelastic behaviour mentioned previously and the relocation of MWCNT after the e-skin subjected to deformation which found in most conductive filling polymer sensor (Liu and Choi, 2014).

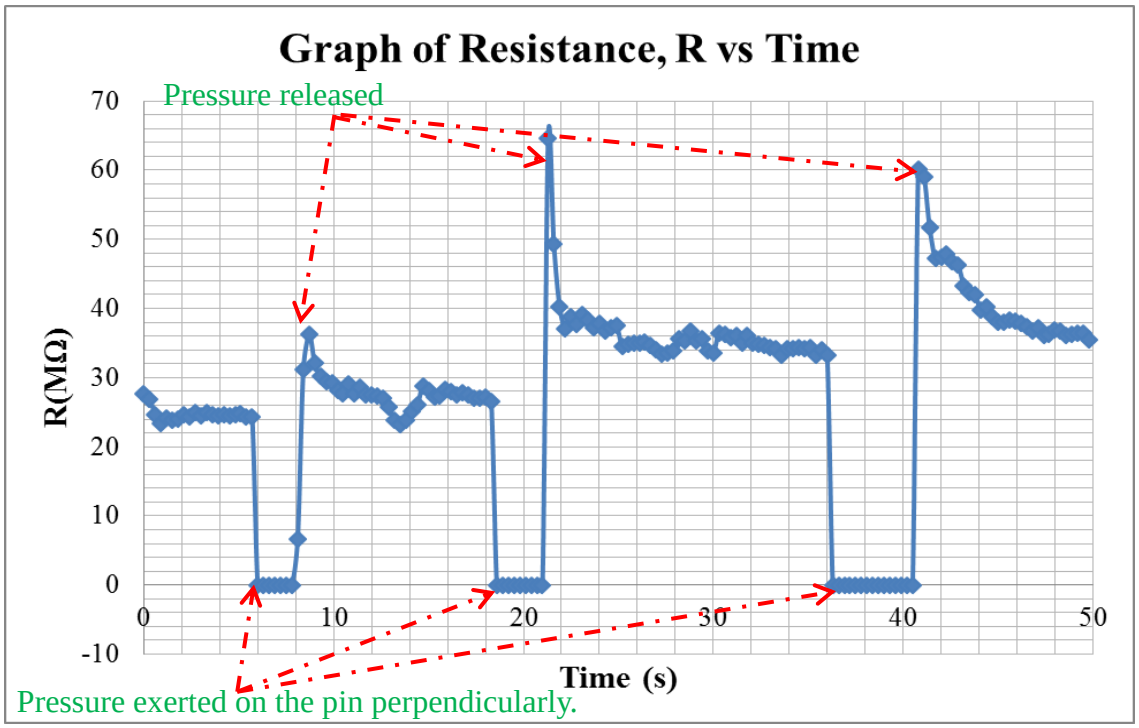

Figure 4.14 Static Response of E-skin

4.5.3 Intensity Mapping

In order to observe the pressure distributed on the e-skin, intensity mapping was done in term of resistance change. The resistance of respective pin was measured and showed in Table 4.1, 4.2 and 4.3 respectively. The results were then normalize to $|\Delta R| / R_o$ and plot using intensity graph in LabVIEW which showed in Figure 4.15. However, due to the uneven surface which mentioned previously owing to some error in the fabrication. The intensity mapping doesn't able to show the shape of object pressed on the e-skin effectively.

Table 4.1: Original Resistance for Respective Pin (all in MΩ)

Top \ Bottom	#2	#3	#4	#5
#2	76.3499	40.7631	33.5216	72.7179
#3	34.7148	16.9225	13.8723	15.6224
#4	33.5897	27.8514	9.8572	19.7512
#5	18.9781	37.0131	15.5684	27.6113

Table 4.2: Resistance for Respective Pin after Loaded (all in MΩ)

Top \ Bottom	#2	#3	#4	#5
#2	51.5659	57.1374	45.4554	65.3668
#3	15.9358	16.7034	10.7894	16.0815
#4	23.1259	27.7739	18.1482	22.3186
#5	29.4799	25.4547	15.4764	32.2810

Table 4.3: |ΔR| / R_o Normalized Resistance

Top \ Bottom	#2	#3	#4	#5
#2	0.3246	0.4017	0.3560	0.1011
#3	0.5410	0.0129	0.2222	0.0294
#4	0.3115	0.0028	0.8411	0.1300
#5	0.5534	0.3123	0.0059	0.1691

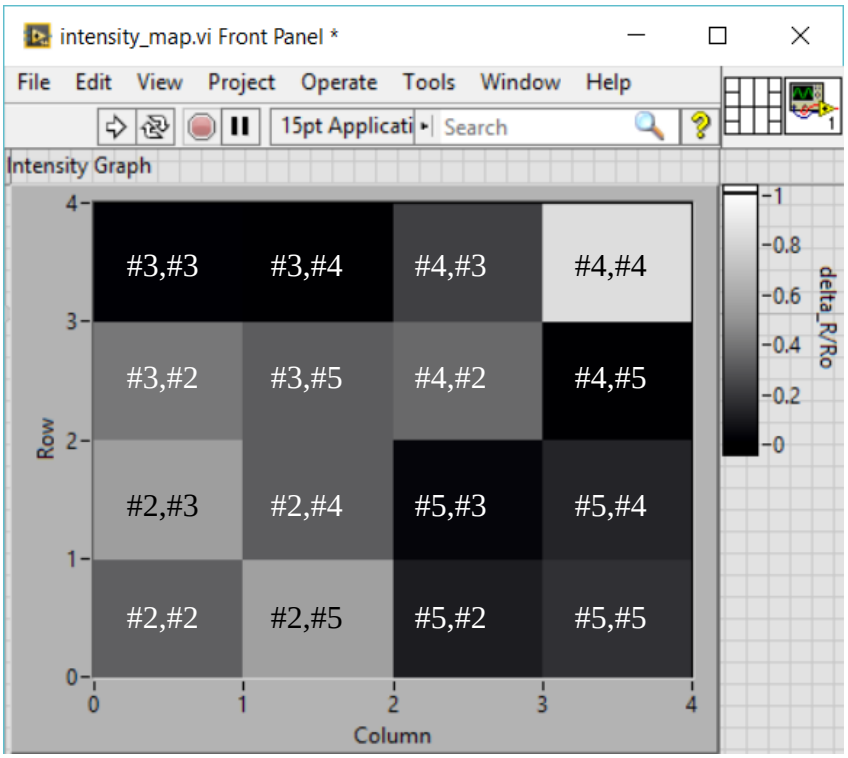

Figure 4.15 Intensity map plot using LabVIEW

4.6 Strain Response

In addition to compressibility, human skin exhibits strain behaviour. Hence, in this experiment, the strain response of the developed e-skin is studied and showed in Figure 4.16. The resistance of the e-skin increases upon pulling the device in y-direction, due to the reallocate MWCNT in the network move further away from

its original position (Alamusi et al., 2011). Hence, the inter-distance of MWCNT increased and the conductivity decreased.

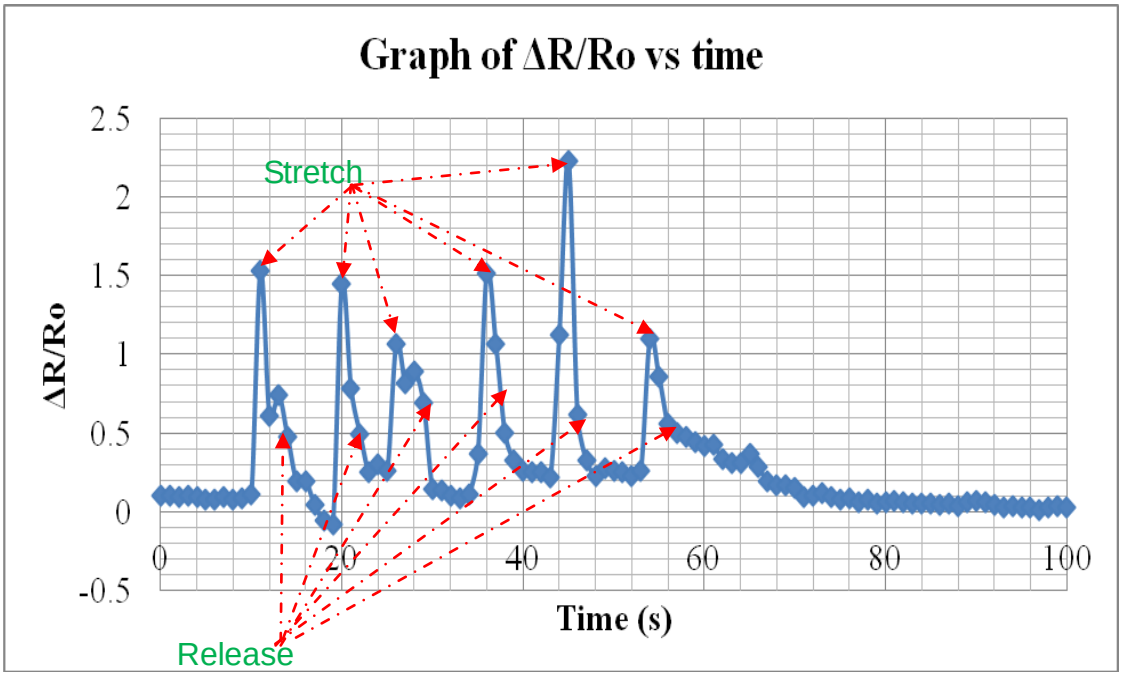

Figure 4.16 Strain Response of E-skin

4.7 Temperature Response

The behaviour of the developed e-skin prototype at different temperature is plotted in Figure 4.17 ranges from 30 °C to 60 °C. The changes of resistance of this prototype shows a negative temperature coefficient (NTC) of resistivity with the slope of $-0.73\ \% K^{-1}$ whereas positive temperature coefficient (PTC) of resistivity behaviour is showed in pure metallic CNT (Chu et al., 2013, Karimov et al., 2011). This is because resistance of the MWCNT/PDMS composite dominates over the resistance change of the MWCNT. Heating up the prototype will result in thermal expansion of the PDMS matrix hence the inter-filler distance between MWCNT is reduced.

To have more accurate measurement, an op-amp can be implemented in linearizing the temperature response (Karimov et al., 2011). Therefore, temperature may change linearly with the resistance. This feature is crucial in temperature

compensation so that additional signal conditioning electronics can be omitted. Hence, the temperature effect can be calibrated by using offset calibration or Wheatstone bridge configuration (Morteza et al., 2015). Besides, it also can be used for temperature sensing without the need of signal conditioning circuit.

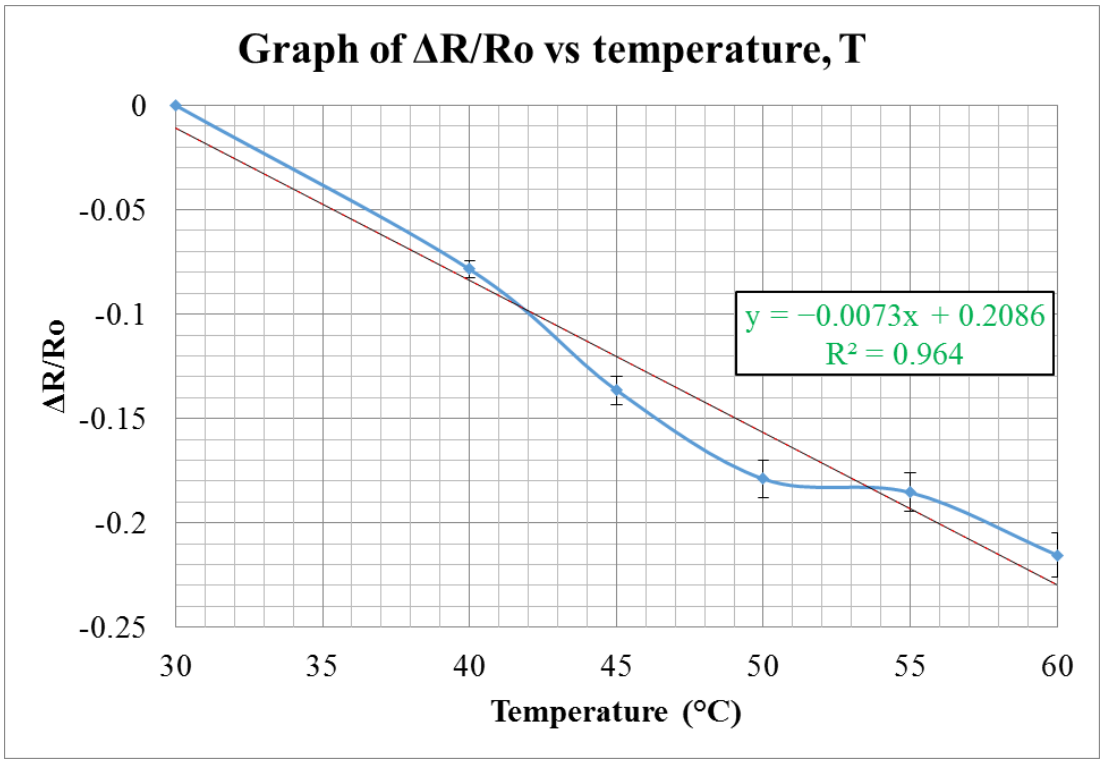

Figure 4.17 Temperature Response of E-skin

CHAPTER 5

CONCLUSION AND RECOMMENDATIONS

5.1 Conclusion

In a nutshell, a stretchable elastomer electronic skin based on piezoresistive mechanism has been developed. The change in piezoresistance of the developed e-skin was able to be measured within the range of 100 MΩ by using DMM of NI ELVIS II+ board. Besides, the fabricated e-skin shows a successfully detection of static and dynamic compressibility pressure, temperature and stretchable strain. Intensity mapping has been performed to show the localised pressure distribution of the e-skin surface. Hence, the objectives outlined in this project have been achieved. Moreover, the developed e-skin could be integrated with robotic arm which allow it to sense touch, temperature and strain.

5.2 Future Works

To enhance the performance of the fabricated device, a bifurcation microstructure can be integrated within the e-skin to have better performance compares to current fabricated prototype. This justification is based on the successfully demonstration of microdome structure in the literature at which the sensitivity of the sensor was improved (Park et al., 2014a, Park et al., 2014b, Park et al., 2015, Hasan et al., 2016). The bifurcation structure mold is proposed to be

printed out using the 3D printing technique, a bifurcation structure mold will be able to be printed out and its structural design. To show the proof of concept, FEA has been performed to investigate the deflection profile and the von Mises stress distribution.

5.2.1 Bifurcation Structural Design

Bifurcation structure is inspired from tilted microdome structure which done by Hasan et al. (Hasan et al., 2016). FEA was carried out for comparison with bifurcation and microdome. The result which studied on the degree of directional deflection for bifurcation is further discussed in next section.

5.2.2 FEA Results

The geometrical of the micropillar and bifurcation are with the cross-sectional area of 2×10^{-10} m. Besides, the dimension for all the structure simulation is tabulated in Table 5.1.

The first comparison is by comparing in the results obtained from Figure 5.1 and Figure 5.2 which are microdome and bifurcation respectively. Then, second comparison is done by comparing the Figure 5.2 and Figure 5.3 which are bifurcation structure with different tip width. After that, comparison of Figure 5.2 and Figure 5.4 are made with bifurcation model of edges and smoothen surface respectively. Finally, the bifurcation structure showed in Figure 5.5 is compared with structure in Figure 5.4 in term of tilting angle.

In the first comparison, von Mises stress which experienced by micropillar and bifurcation are more or less the same, but bifurcation showed a two degree of shear force deflection due to the Y-shaped tips. The second comparison shows that the shorter tip width of bifurcation structure experience higher von Mises stress

however, the pressure is distributed more uniformly at bigger region. For the third comparison, the bifurcation structure with smoothen edge experiences more evenly distribute and lesser von Mises stress than its counterpart. In conclusion, the bifurcation structure in Figure 5.5 is chosen due to fabrication constraint and longer lasting as lesser von Mises stress experienced by the structure.

Table 5.1: Dimension Listing for Designed Structures

Structure	Dimension (μm)			Inclination Degree (◦)
	Diameter, d / Tip width, t	Height, h	Pitch, p	
Figure 5.1	13.0	16.0	-	-
Figure 5.2	5.0	20.0	-	60.0
Figure 5.3	8.5	17.1	-	60.0
Figure 5.4	7.2	20.0	-	60.0
Figure 5.5	50.0	200.0	200.0	11.7

* Diameter only applicable for micropillar and tip width for bifurcation

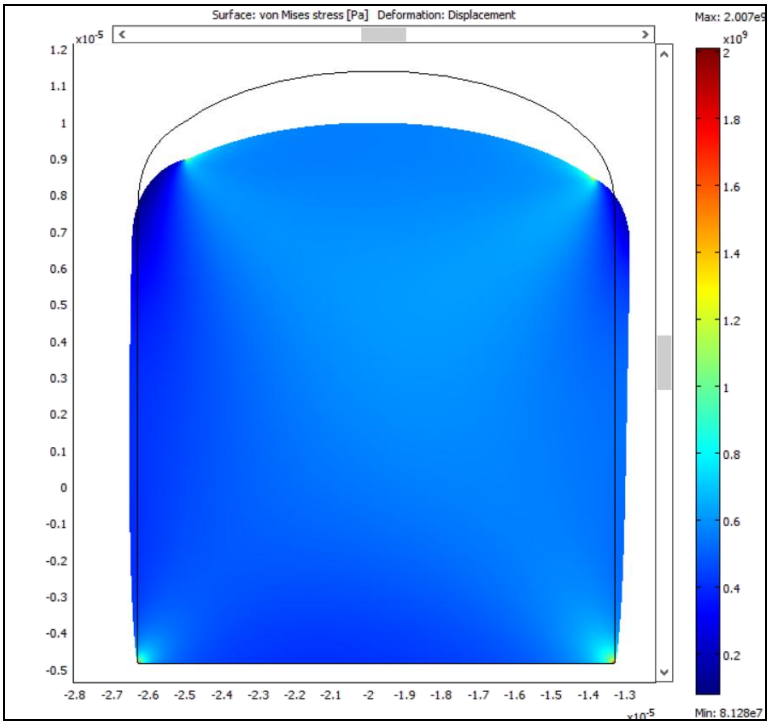

Figure 5.1 FEA on Micropillar Structure

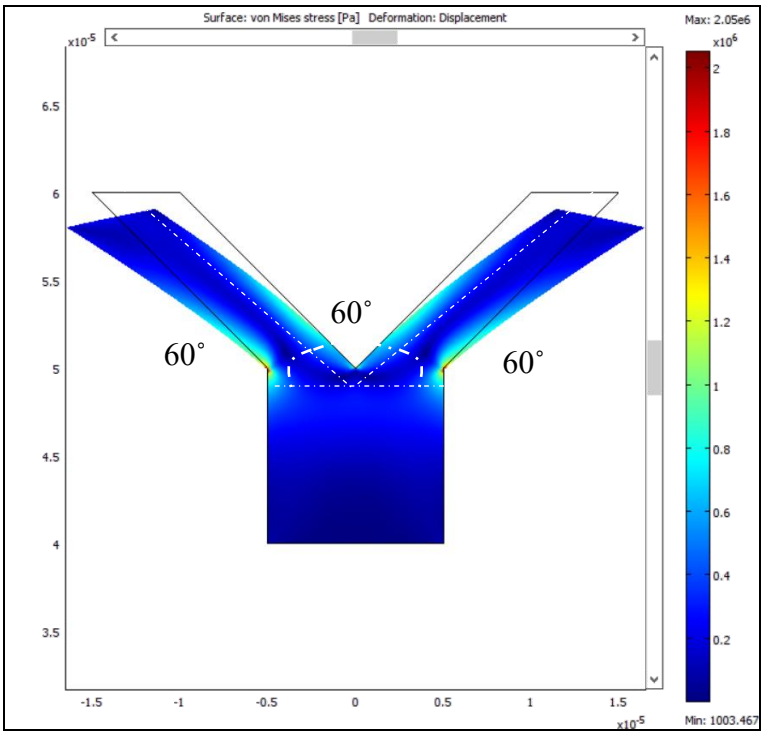

Figure 5.2 FEA on Bifurcation with 60° Tilting Angle (Thin Sharp Tip)

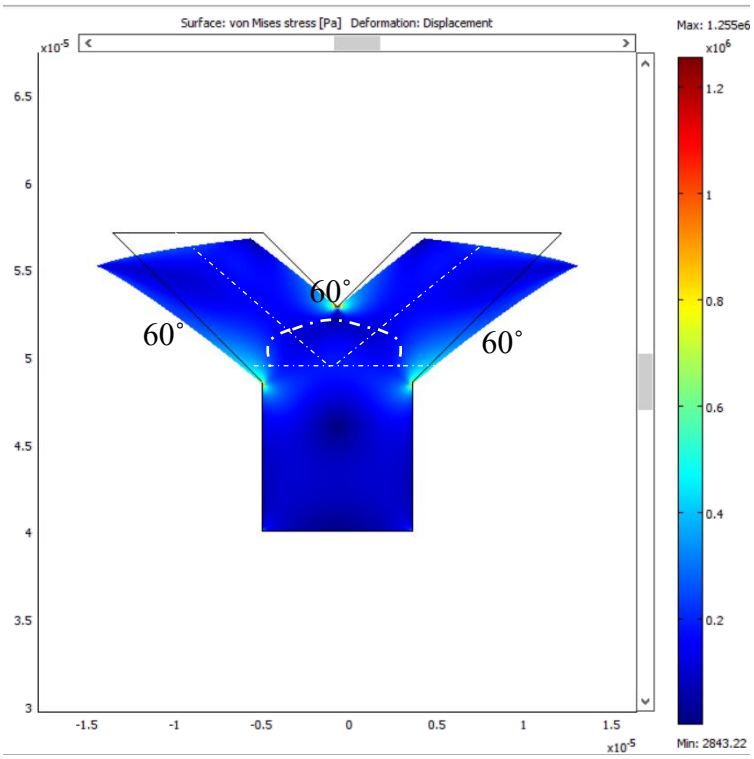

Figure 5.3 FEA on Bifurcation with 60° Tilting Angle (Thick Sharp Tip)

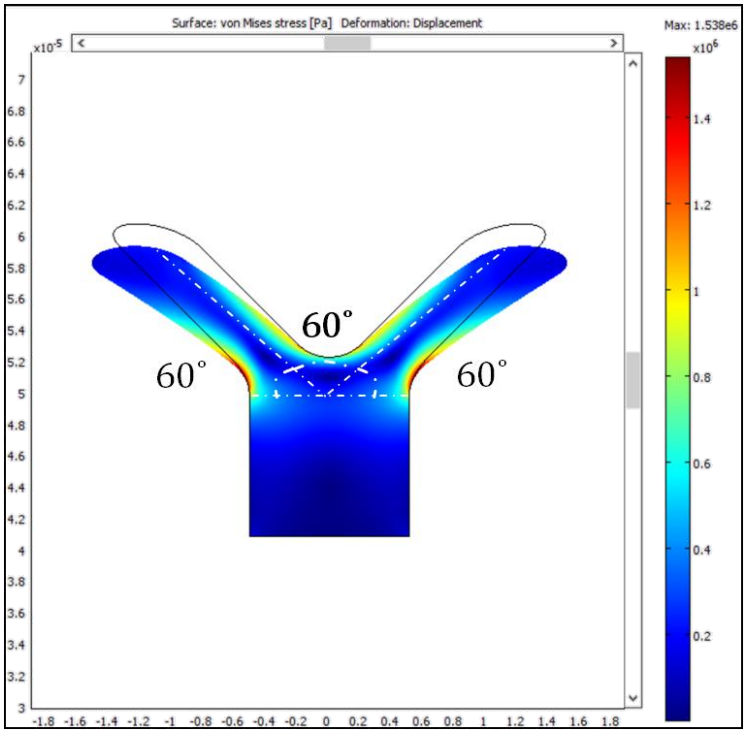

Figure 5.4 FEA on Bifurcation with 60° Tilting Angle (Smoothen Edge)

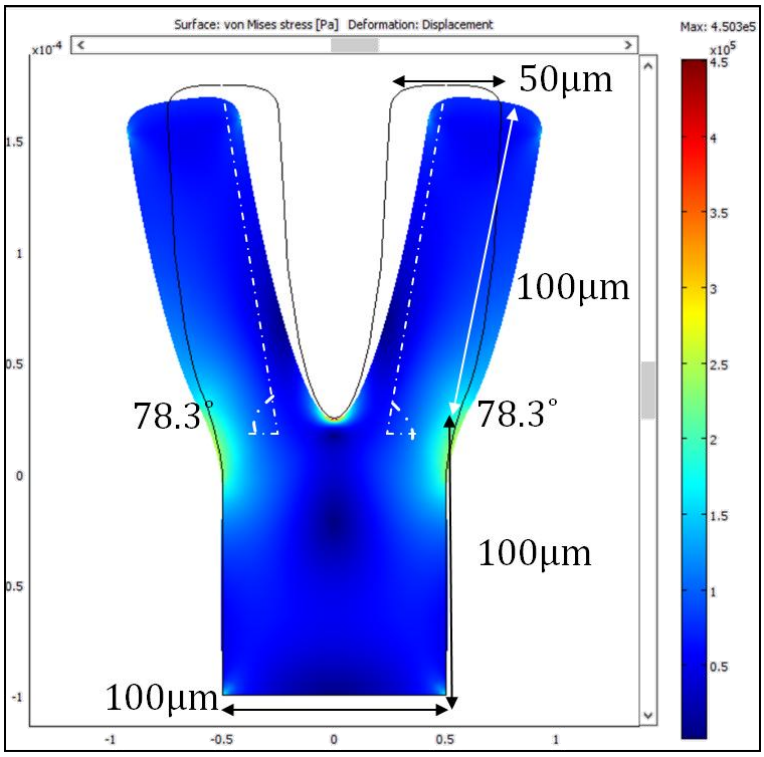

Figure 5.5 FEA on Finalized Bifurcation with 78.3° Tilting Angle

REFERENCES

Alamusi, Hu, N., Fukunaga, H., Atobe, S., Liu, Y. & Li, J. 2011. Piezoresistive Strain Sensors Made from Carbon Nanotubes Based Polymer Nanocomposites. *Sensors (Basel, Switzerland),* 11**,** 10691-10723.

Andersw 2008. *COMSOL Multiphysics User's Guide,* COMSOL AB.

Bokobza, L. 2007. Multiwall carbon nanotube elastomeric composites: A review. *Polymer,* 48**,** 4907-4920.

Chu, K., Kim, D., Sohn, Y., Lee, S., Moon, C. & Park, S. 2013. Electrical and Thermal Properties of Carbon-Nanotube Composite for Flexible Electric Heating-Unit Applications. *IEEE Electron Device Letters,* 34**,** 668-670.

Communications, T. 2009. NI ELVIS II series specifications - national instruments.

Fan-Gang, T., Chih-Sheng, Y. & Li-Chern, P. An elastomeric tactile sensor employing dielectric constant variation and applicable to orthodontia. Micro Electro Mechanical Systems, 2004. 17th IEEE International Conference on. (MEMS), 2004 2004. 564-567.

Firouzeh, A., Foba Amon-Junior, A. & Paik, J. 2015. Soft piezoresistive sensor model and characterization with varying design parameters. *Sensors and Actuators A: Physical,* 233**,** 158-168.

Hammock, M. L., Chortos, A., Tee, B. C. K., Tok, J. B. H. & Bao, Z. 2013. 25th Anniversary Article: The Evolution of Electronic Skin (E-Skin): A Brief History, Design Considerations, and Recent Progress. *Advanced Materials,* 25**,** 5997-6038.

"The Six Million dollar man" (1974), 2002. Directed by Harve, B. USA: American Broadcasting Company (ABC).

Hasan, S., Jung, Y., Kim, S., Jung, C.-L., Oh, S., Kim, J. & Lim, H. 2016. A Sensitivity Enhanced MWCNT/PDMS Tactile Sensor Using Micropillars and Low Energy Ar+ Ion Beam Treatment. *Sensors,* 16**,** 93.

Hutton, D. V. 2004. *Fundamentals of Finite Element Analysis,* McGraw-Hill.

Instruments, N. 2012. LabVIEW system design software - national instruments.

Karimov, K. S., Chani, M. T. S. & Khalid, F. A. 2011. Carbon nanotubes film based temperature sensors. *Physica E: Low-dimensional Systems and Nanostructures,* 43**,** 1701-1703.

Khosla, A. & Gray, B. L. 2009. Preparation, characterization and micromolding of multi-walled carbon nanotube polydimethylsiloxane conducting nanocomposite polymer. *Materials Letters,* 63**,** 1203-1206.

Kubo, M., Li, X., Kim, C., Hashimoto, M., Wiley, B. J., Ham, D. & Whitesides, G. M. 2010. Stretchable Microfluidic Radiofrequency Antennas. *Advanced Materials,* 22**,** 2749-2752.

Lacour, S. P., Wagner, S., Huang, Z. & Suo, Z. 2003. Stretchable gold conductors on elastomeric substrates. *Applied Physics Letters,* 82**,** 2404-2406.

Liu, C.-X. & Choi, J.-W. 2012. Improved Dispersion of Carbon Nanotubes in Polymers at High Concentrations. *Nanomaterials,* 2**,** 329.

Liu, C.-X. & Choi, J.-W. 2014. Analyzing resistance response of embedded PDMS and carbon nanotubes composite under tensile strain. *Microelectronic Engineering,* 117**,** 1-7.

Liu, C. 2011. *Foundations of MEMS,* Prentice Hall Press.

Livermore, C. 2004. *PDMS* [Online]. 6.777J/2.751J Material Properties Database. Available: http://www.mit.edu/~6.777/matprops/pdms.htm [Accessed].

Lu, N., Lu, C., Yang, S. & Rogers, J. 2012. Highly Sensitive Skin-Mountable Strain Gauges Based Entirely on Elastomers. *Advanced Functional Materials,* 22**,** 4044-4050.

Mark, J. E. 1999. *Polymer Data Handbook,* Oxford University Press.

Morteza, A., Yong Jin, Y. & Inkyu, P. 2015. Ultra-stretchable and skin-mountable strain sensors using carbon nanotubes–Ecoflex nanocomposites. *Nanotechnology,* 26**,** 375501.

Pang, C., Lee, G.-Y., Kim, T.-I., Kim, S. M., Kim, H. N., Ahn, S.-H. & Suh, K.-Y. 2012. A flexible and highly sensitive strain-gauge sensor using reversible interlocking of nanofibres. *Nat Mater,* 11**,** 795-801.

Park, J., Kim, M., Lee, Y., Lee, H. S. & Ko, H. 2015. Fingertip skin–inspired microstructured ferroelectric skins discriminate static/dynamic pressure and temperature stimuli. *Science Advances,* 1.

Park, J., Lee, Y., Hong, J., Ha, M., Jung, Y.-D., Lim, H., Kim, S. Y. & Ko, H. 2014a. Giant Tunneling Piezoresistance of Composite Elastomers with Interlocked Microdome Arrays for Ultrasensitive and Multimodal Electronic Skins. *ACS Nano,* 8**,** 4689-4697.

Park, J., Lee, Y., Hong, J., Lee, Y., Ha, M., Jung, Y., Lim, H., Kim, S. Y. & Ko, H. 2014b. Tactile-Direction-Sensitive and Stretchable Electronic Skins Based on Human-Skin-Inspired Interlocked Microstructures. *ACS Nano,* 8**,** 12020-12029.

Park, J., Lee, Y., Lim, S., Lee, Y., Jung, Y., Lim, H. & Ko, H. 2014c. Ultrasensitive Piezoresistive Pressure Sensors Based on Interlocked Micropillar Arrays. *BioNanoScience,* 4**,** 349-355.

Shilalla 2006. 5800 series brochure.

Tai, Y.-L. & Yang, Z.-G. 2015. Flexible pressure sensing film based on ultra-sensitive SWCNT/PDMS spheres for monitoring human pulse signals. *Journal of Materials Chemistry B,* 3**,** 5436-5441.

Tang, Q.-Y., Pan, Y.-M., Chan, Y. C. & Leung, K. W. 2012. Frequency-tunable soft composite antennas for wireless sensing. *Sensors and Actuators A: Physical,* 179**,** 137-145.

Zhang, M., Wu, J., Wang, L., Xiao, K. & Wen, W. 2010. A simple method for fabricating multi-layer PDMS structures for 3D microfluidic chips. *Lab on a Chip,* 10**,** 1199-1203.

Zhang, Y., Wang, S., Li, X., Fan, J. A., Xu, S., Song, Y. M., Choi, K.-J., Yeo, W.-H., Lee, W., Nazaar, S. N., Lu, B., Yin, L., Hwang, K.-C., Rogers, J. A. & Huang, Y. 2014. Experimental and Theoretical Studies of Serpentine Microstructures Bonded To Prestrained Elastomers for Stretchable Electronics. *Advanced Functional Materials,* 24**,** 2028-2037.

Zhang, Y., Xu, S., Fu, H., Lee, J., Su, J., Hwang, K.-C., Rogers, J. A. & Huang, Y. 2013. Buckling in serpentine microstructures and applications in elastomer-supported ultra-stretchable electronics with high areal coverage. *Soft Matter,* 9**,** 8062-8070.